Protein Detection by Sequencing
Uncover What Makes Each Cell Unique With Antibodies, Panels, and Multiomics Software
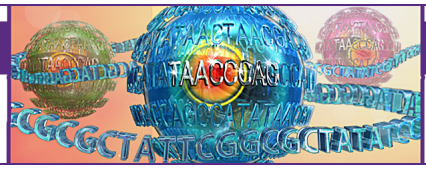
BioLegend®
Learn More

The Journal of Immunology

This information is current as of April 20, 2021.

Phenotypic and Clonal Stability of Antigen-Inexperienced Memory-like T Cells across the Genetic Background, Hygienic Status, and Aging

Alena Moudra, Veronika Niederlova, Jiri Novotny, Lucie Schmiedova, Jan Kubovciak, Tereza Matejkova, Ales Drobek, Michaela Pribikova, Romana Stopkova, Dagmar Cizkova, Ales Neuwirth, Juraj Michalik, Katerina Krizova, Tomas Hudcovic, Michal Kolar, Hana Kozakova, Jakub Kreisinger, Pavel Stopka and Ondrej Stepanek

J Immunol 2021; 206:2109-2121; Prepublished online 15 April 2021;
doi: 10.4049/jimmunol.2001028
http://www.jimmunol.org/content/206/9/2109

Supplementary Material http://www.jimmunol.org/content/suppl/2021/04/15/jimmunol.2001028.DCSupplemental

References This article **cites 49 articles**, 20 of which you can access for free at:
http://www.jimmunol.org/content/206/9/2109.full#ref-list-1

Why *The JI*? Submit online.

- **Rapid Reviews! 30 days*** from submission to initial decision
- **No Triage!** Every submission reviewed by practicing scientists
- **Fast Publication!** 4 weeks from acceptance to publication

**average*

Subscription Information about subscribing to *The Journal of Immunology* is online at:
http://jimmunol.org/subscription

Permissions Submit copyright permission requests at:
http://www.aai.org/About/Publications/JI/copyright.html

Email Alerts Receive free email-alerts when new articles cite this article. Sign up at:
http://jimmunol.org/alerts

The Journal of Immunology is published twice each month by
The American Association of Immunologists, Inc.,
1451 Rockville Pike, Suite 650, Rockville, MD 20852
Copyright © 2021 by The American Association of Immunologists, Inc. All rights reserved.
Print ISSN: 0022-1767 Online ISSN: 1550-6606.

Downloaded from http://www.jimmunol.org/ at Institute of Physiology ASCR on April 20, 2021

Phenotypic and Clonal Stability of Antigen-Inexperienced Memory-like T Cells across the Genetic Background, Hygienic Status, and Aging

Alena Moudra,*,[1] Veronika Niederlova,* Jiri Novotny,[†,‡] Lucie Schmiedova,[§] Jan Kubovciak,[†,§] Tereza Matejkova,[¶] Ales Drobek,* Michaela Pribikova,*,[‖] Romana Stopkova,[¶] Dagmar Cizkova,[#] Ales Neuwirth,* Juraj Michalik,* Katerina Krizova,* Tomas Hudcovic, Michal Kolar,[†,‡] Hana Kozakova,** Jakub Kreisinger,[§] Pavel Stopka,[¶] and Ondrej Stepanek*,[††]**

Ag-inexperienced memory-like T (AIMT) cells are functionally unique T cells, representing one of the two largest subsets of murine CD8$^+$ T cells. However, differences between laboratory inbred strains, insufficient data from germ-free mice, a complete lack of data from feral mice, and an unclear relationship between AIMT cells formation during aging represent major barriers for better understanding of their biology. We performed a thorough characterization of AIMT cells from mice of different genetic background, age, and hygienic status by flow cytometry and multiomics approaches, including analyses of gene expression, TCR repertoire, and microbial colonization. Our data showed that AIMT cells are steadily present in mice, independent of their genetic background and hygienic status. Despite differences in their gene expression profiles, young and aged AIMT cells originate from identical clones. We identified that CD122 discriminates two major subsets of AIMT cells in a strain-independent manner. Whereas thymic CD122^{LOW} AIMT cells (innate memory) prevail only in young animals with high thymic IL-4 production, peripheral CD122^{HIGH} AIMT cells (virtual memory) dominate in aged mice. Cohousing with feral mice changed the bacterial colonization of laboratory strains but had only minimal effects on the CD8$^+$ T cell compartment, including AIMT cells. ***The Journal of Immunology*****, 2021, 206: 2109–2121.**

Antigen-inexperienced memory-like T (AIMT) cells are divided into two subsets based on the site of their origin. Innate T cells originate in the thymus, whereas virtual memory T cells are formed in the peripheral lymphoid organs (1, 2). In BALB/c (BALB) mice and several gene knockouts on C57BL/6 (B6) background, innate memory cells are formed in the

*Laboratory of Adaptive Immunity, Institute of Molecular Genetics of the Czech Academy of Sciences, Prague, Czech Republic; [†]Laboratory of Genomics and Bioinformatics, Institute of Molecular Genetics of the Czech Academy of Sciences, Prague, Czech Republic; [‡]Department of Informatics and Chemistry, Faculty of Chemical Technology, University of Chemistry and Technology, Prague, Czech Republic; [§]Department of Zoology, Faculty of Science, Charles University, Prague, Czech Republic; [¶]Department of Zoology, Faculty of Science, BIOCEV, Charles University, Vestec, Czech Republic; [‖]Laboratory of Immunity & Cell Communication, First Faculty of Medicine, BIOCEV, Charles University, Vestec, Czech Republic; [#]Research Facility Studenec, Institute of Vertebrate Biology, Czech Academy of Sciences, Brno, Czech Republic; **Laboratory of Gnotobiology, Institute of Microbiology of the Czech Academy of Sciences, Novy Hradek, Czech Republic; and [††]Department of Biomedicine, University Hospital and University of Basel, Basel, Switzerland

[1]Current address: Laboratory of Lymphocyte Signalling and Development, The Babraham Institute, Cambridge, United Kingdom

ORCIDs: 0000-0003-3465-7812 (A.M.); 0000-0001-8768-9039 (V.N.); 0000-0003-1338-638X (J.N.); 0000-0003-2180-5281 (L.S.); 0000-0001-6446-9797 (J. Kubovciak); 0000-0003-0154-4264 (T.M.); 0000-0003-1066-9413 (A.D.); 0000-0001-8331-3923 (R.S.); 0000-0001-5031-7792 (D.C.); 0000-0003-4668-4316 (A.N.); 0000-0002-5320-4504 (T.H.); 0000-0002-4593-1525 (M.K.); 0000-0001-7352-5922 (H.K.); 0000-0002-1104-1655 (P.S.); 0000-0002-2735-3311) (O.S.).

Received for publication November 9, 2020. Accepted for publication March 1, 2021.

This work was supported by the Czech Science Foundation (19-03435Y to O.S., 18-17796Y to J. Kreisinger, 19-02261S to H.K.), the Swiss National Science Foundation (IZ11Z0_166538 to O.S.), and the European Research Council (FunDiT to O.S.). The Laboratory of Adaptive Immunity was supported by a European Molecular Biology Organization Installation grant (3259 to O.S.). The Laboratory of Adaptive Immunity and the Laboratory of Genomics and Bioinformatics were supported by Institute of Molecular Genetics of the Czech Academy of Sciences core funding (RVO 68378050). O.S. was supported by the Czech Academy of Sciences, which provided a Purkyne Fellowship. P.S., R.S., and T.M. were supported by funding from the European Union Horizon 2020 Framework Programme to the MICOBION project (810224). J.N. and M.K. were supported by funds provided by the Czech Ministry of Education, Science, Research and Sport of the Slovak Republic to the Center for Tumor Ecology–Research of the Cancer Microenvironment Supporting Cancer Growth and Spread (OP RDI CZ.02.1.01/0.0/0.0/16_019/0000785). L.S. was supported by the Charles University specific research grant (SVV 260571/2020). A.M. and V.N. were students partially supported by the Faculty of Science, Charles University, Prague. J.N. was a student partially supported by the University of Chemistry and Technology, Prague. The animal facility of the Institute of Molecular Biology of the Czech Academy of Sciences is a part of the Czech Centre for Phenogenomics, and the work there was supported in part by the following grants: LM2015040, LM2018126, OP RDI CZ.1.05/2.1.00/19.0395, OP RDI BIOCEV CZ.1.05/1.1.00/02.0109 provided by the Czech Ministry of Education, Youth and Sports and the European Regional Development Fund.

A.M. performed most of the experiments. V.N., L.S., M.P., A.D., R.S., T.M., A.N., K.K., P.S., and O.S. performed experiments. A.M., V.N., and O.S. analyzed data and finalized figures. J. Kubovciak and J.M. analyzed the transcriptomic data. J.N. analyzed the TCR-profiling data. D.C. and J. Kreisinger analyzed the S16-sequencing data. R.S. and P.S. provided feral mice. T.H. and H.K. provided germ-free mice. M.K., H.K., J. Kreisinger, P.S., and O.S. supervised the work. O.S. conceived the study. A.M., V.N., and O.S. wrote the manuscript. All the authors contributed to the manuscript and reviewed it.

The transcriptomic data files presented in this article have been submitted to the Array Express database (www.ebi.ac.uk/arrayexpress) under accession number E-MTAB-9091. The TCR sequence data have been submitted to the Sequence Read Archive and BioProject databases at the National Center for Biotechnology Information under accession number PRJNA633838 (https://www.ncbi.nlm.nih.gov/bioproject/PRJNA633838). The bacterial S16-sequencing data have been submitted to the European Nucleotide Archive under accession PRJEB38301. Health monitoring data relating to this article have been submitted to Zenodo (https://zenodo.org/record/4298697#.YGxxu2RKhts).

Address correspondence and reprint requests to Ondrej Stepanek, Laboratory of Adaptive Immunity, Institute of Molecular Genetics of the Czech Academy of Sciences, Videnska 1083, 14220 Prague, Czech Republic. E-mail ondrej.stepanek@img.cas.cz

The online version of this article contains supplemental material.

Abbreviations used in this article: AgE, Ag-experienced; AIMT, Ag-inexperienced memory-like T; B6, C57BL/6; BALB, BALB/c; DO11.10, C.Cg-Tg(DO11.10)10Dlo/J; F1, first generation; iNKT, invariant NKT; PCA, principal component analysis; SPF, specific pathogen–free; WT, wild-type.

Copyright © 2021 by The American Association of Immunologists, Inc. 0022-1767/21/$37.50

Downloaded from http://www.jimmunol.org/ at Institute of Physiology ASCR on April 20, 2021

thymus via IL-4 produced by invariant NKT (iNKT) cells (3–5). Wild-type (WT) B6 mice have low numbers of IL-4–producing iNKT cells in the thymus and form virtual memory T cells in a process dependent of IL-15 presentation by peripheral CD8α dendritic cells (2, 5–7). Recently, it has been observed that mature $CD8^+$ single-positive thymic precursors of virtual memory T cells upregulate Eomes (8), a transcription factor required for their existence (7), suggesting that the differentiation process of virtual memory cells might be initiated already in the thymus and accomplished in the periphery (9). This scenario is consistent with the observation that thymocytes developing in a neonatal thymus are more predisposed toward AIMT cell formation than thymocytes developing in an adult thymus of B6 mice (10).

In addition to these major routes, lymphopenia induces homeostatic proliferation coupled with the differentiation of peripheral naive $CD8^+$ T cells into AIMT cells, probably via IL-7 and/or IL-15 in B6 mice (11, 12). Moreover, an excess of IL-4, IL-7, or IL-15 induces the formation and/or expansion of AIMT cells (6, 13, 14). Given the fact that these three cytokines signal through the common γ-chain (15), it is not surprising that all of them induce AIMT cell formation. Although it has been proposed that some genes, such as *Tbx21*/T-bet or *Klrk1*/NKG2D, are differentially expressed in thymic innate memory and virtual memory AIMT cells (2), a direct comparison of the gene expression between virtual memory and innate memory T cells has not been carried out.

Despite their abundance and functional uniqueness, AIMT cells are still understudied. The potential reasons for the underrepresentation of AIMT cells in the immunological research could be the confusing nomenclature (1) and unclear developmental and functional relationship between different types of AIMT cells. Moreover, only a minority of AIMT cell-related studies used germ-free mice (8, 16, 17), which might obscure the interpretation of the observations. It is unclear whether the very existence of AIMT cells is physiological because AIMT cells have been characterized exclusively in inbred mouse strains housed in clean conditions and because it has been proposed that the $CD8^+$ T cell compartment in laboratory mice substantially differs from feral mice (18).

In this study, we show in side-by-side controlled experiments for the first time, to our knowledge, that the routes of AIMT cell formation are conserved in mice with different genetic backgrounds and hygienic conditions, including germ-free and feral mice.

Materials and Methods

Ab

The Absthat were used for flow cytometry were purchased from BD Pharmingen and included the following: CD4 PE-Cy7 (RM4-5), catalog no. 552775; CD4 allophycocyanin-Cy7 (GK1.5), catalog no. 552051; CD4 Alexa Fluor 700 (RM4-5), catalog no. 557956; CD4 FITC (H129.19), catalog no. 553651; CD8α Pacific Blue (53-6.7), catalog no. 558106; CD49d PE (R1-2), catalog no. 553157; Ki67 Alexa Fluor 647 (B56), catalog no. 558615; KLRG1 allophycocyanin (2F1/KLRG1), catalog no. 553157; Ly-6c FITC (MR5-2), catalog no. 553186; TCR Vα2 PE (B20.1), catalog no. 553289; TCR Vα8.3 FITC (B21.14), catalog no. 553376; TCR Vβ8.1/8.2 FITC (MR5-2), catalog no. 553185; TCRβ allophycocyanin (H57-597), catalog no. 553174; and TCRβ PE (H57-597), catalog no. 553171. The following Abs were from BioLegend: CD4 Brilliant Violet 650 (RM4-5), catalog no. 100545; CD5 Brilliant Violet 510 (53-7-3), catalog no. 100627; CD8α Brilliant Violet 421 (53-6.7), catalog no. 558106; CD8α Brilliant Violet 510 (53-6.7), catalog no. 558106; CD24 FITC (M1/69), catalog no. 101806; CD44 Brilliant Violet 650 (IM7), catalog no. 103049; CD44 PerCP-Cy5.5 (IM7), catalog no. 103032; CD49d PE-Cy7 (R1-2), catalog no. 103618; CD62L Alexa Fluor 700 (MEL14), catalog no. 104426; CD122 FITC (TM-β1), catalog no. 123207; CD127 PE-Cy7 (A7R34), catalog no. 135015; CD127 PE (A7R34), catalog no. L34975; CD218a Alexa Fluor 647 (BG/IL18RA), catalog no. 132903; CX3CR1 PE-Cy7 (SA011F11), catalog no. 149016; IFN-γ Alexa Fluor 700 (XMG1.2), catalog no. 505824; TCR Vα8.3 PE (B21.14), catalog no. 127708; and TCR γ/δ PerCP-Cy5.5 (GL3), catalog no. 118117. Abs from eBioscience included the following: CD122 PerCP–eFluor 710 (TM-β1), catalog no. 46-1222-80; and EOMES Alexa Fluor 488 (Dan11mag), catalog no. 53-4875-80.

Laboratory mice

Common laboratory mouse strains C57BL/6J and BALB and transgenic mouse strains Vβ5 (19) and C.Cg-Tg(DO11.10)10Dlo/J (DO11.10) (20) were used in this study.

Mice were bred in our facilities (specific pathogen–free [SPF] mice at the Institute of Molecular Genetics of the Czech Academy of Sciences, Prague, Czech Republic and the Department of Biomedicine, University Hospital Basel, Basel, Switzerland; germ-free mice at the Laboratory of Gnotobiology, Institute of Microbiology of the Czech Academy of Sciences, Novy Hradek, Czech Republic) in accordance with laws of the Czech Republic and Switzerland, respectively. Animal protocols were approved by the Cantonal Veterinary Office of Baselstadt, Switzerland, by the Czech Academy of Sciences, the Czech Republic, and by the respective Committees for the Protection and Use of Experimental Animals of the Institute of Microbiology (identification no. 5/2019) and of the Institute of Molecular Genetics (identification no. 8/2017, 15/2019) of the Czech Academy of Sciences.

Mice were kept in the animal facility with a 12 h of light–dark cycle with food and water ad libitum. Males and females were used for experiments. Age- and sex-matched pairs of animals were used in the experimental groups. If possible, littermates were equally divided into the experimental groups.

Flow cytometry and cell counting

For the surface staining, cells were incubated with diluted Abs in PBS/2% FCS on ice. LIVE/DEAD Near-IR dye (Life Technologies, L34975) was used for discrimination of live and dead cells.

For the staining of feral mice, cohoused mice, and control animals, cells were fixed with 2% formaldehyde at room temperature for 3 min prior to staining. All monoclonal Abs used for this staining were tested for their compatibility with the fixation procedure.

For intracellular staining, cells were fixed and permeabilized using Foxp3/Transcription Factor Staining Buffer Set (00-5523-00; eBioscience). For some experiments, enrichment of $CD8^+$ T cells was performed using EasySep Magnetic bead separation kits (STEMCELL Technologies) or Dynabeads (Thermo Fisher Scientific), according to manufacturers' instructions, prior to the analysis or sorting by flow cytometry.

Cells were counted using a Z2 Particle Counter (Beckman Coulter) or using AccuCheck Counting beads (Thermo Fisher Scientific) and a flow cytometer. Flow cytometry was carried out with BD LSR II, BD FACSCanto II, or Cytek Aurora cytometers. Cell sorting was performed using BD Influx (BD Biosciences). Data were analyzed using FlowJo software (Tree Star).

Stimulation of T cells

A total of 400,000 cells/ml freshly isolated lymph node cells in IMDM/10% FCS supplemented with IL-2 were stimulated with PMA (10 ng/ml) and ionomycin (1 μM) or IL-12 (10 ng/ml) and IL-18 (10 ng/ml) or left unstimulated for 8 h. A total of 5 μg/ml brefeldin A (420601; BioLegend) was added to the culture for the last four hours of the incubation. The cells were stained with LIVE/DEAD Near-IR dye and fluorescently labeled Abs to CD8α, CD44, and CD49d. After washing, the cells were fixed and permeabilized and labeled with anti–IFN-γ Ab and analyzed by flow cytometry.

Sublethal irradiation

C57BL/6J and BALB mice age 5–8 wk were sublethally irradiated with 4 Gy on a T-200 x-ray machine (WOLF-Medizintechnik). The mice were sacrificed at day 16 postirradiation, and the lymphocytes from the peripheral lymph nodes and the spleen were stained for CD122, CD8α, viability, CD44, CD62L, CD49d, CD4, TCRβ, Ly-6c, and CD5 and analyzed by flow cytometry. The control group consisted of nonirradiated littermates.

Adoptive transfer of cells into DO11.10 mice

Lymphocytes from peripheral lymph nodes and spleen from 8- to 12-wk-old BALB mice were harvested and stained with 5 μM CellTrace Violet proliferation dye (C34557; Thermo Fisher Scientific) in PBS for 10 min at 37°C. A total of 1×10^6 naive $CD8^+$ $CD44^-$ cells were sorted and i.v. injected into recipient DO11.10 mouse. The phenotype of the transferred cells was analyzed after 7 d.

Samples for transcriptomic analysis

Ten- to twelve-week-old BALB or C57BL/6J SPF mice were irradiated with 4 Gy and sacrificed 16 d postirradiation. Nonirradiated mice were young SPF (7–12 wk) or aged (12–19 mo) BALB or C57BL/6J mice.

Downloaded from http://www.jimmunol.org/ at Institute of Physiology ASCR on April 20, 2021

Lymphocytes from the peripheral lymph nodes and the spleen were stained with TCRβ, CD8, CD44, CD49d, CD122, and viability dye and sorted by Influx. Each sample consisted of a pool of lymphocytes originating from 2–5 mice.

RNA was isolated using TRIzol LS (Thermo Fisher Scientific) followed by in-column DNase digestion using RNA a Clean & Concentrator Kit (Zymo Research), according to manufacturers' instructions.

Transcriptomic analysis

Samples were prepared with SMARTer Stranded Total RNA-Seq v2–Pico Input Mammalian library preparation kit (Takara Bio). The protocol included cDNA synthesis from mRNA, ligation of sequencing adaptors and indexes, ribosomal cDNA depletion, final PCR amplification, and product purification. Library size distribution was evaluated on the Agilent 2100 Bioanalyzer using the High Sensitivity DNA Kit (Agilent Technologies). Libraries were sequenced using an Illumina NextSeq 500 instrument using 76-bp single-end high-output configuration.

Read quality was assessed by FastQC (http://www.bioinformatics.babraham.ac.uk/projects/fastqc). For subsequent read processing, a bioinformatics pipeline nf-core/rnaseq version 1.1 (https://doi.org/10.5281/zenodo.1447331), was used. Individual steps included removing sequencing adaptors with Trim Galore! (http://www.bioinformatics.babraham.ac.uk/projects/trim_galore/), mapping to reference genomes GRCm38 or BALB _cJ_v1 (21) (Ensembl annotation version 94) respective to the specimen strain with HISAT2 (22), and quantifying expression on gene level with featureCounts (23). Resulting per gene read counts for individual strains were merged together using a gene ortholog map obtained from Ensembl. Merged counts served as input for differential expression analysis using DESeq2 R Bioconductor package (24). Prior to the analysis, genes not expressed in at least two samples were discarded. Shrunken $\log_2$-fold changes using the adaptive shrinkage estimator (25) were used for differential expression analysis. Genes exhibiting minimal absolute $\log_2$-fold change value of 1 and statistical significance of adjusted p value <0.05 between compared groups of samples were considered as differentially expressed for subsequent interpretation and visualization.

To show sample expression relatedness with the generic effect of mouse strain erased, we employed a method of removing unwanted source of variation by fitting a linear model using the limma R Bioconductor package (26) (function removeBatchEffect) after normalizing the data using variance-stabilizing transformation.

Raw fastq files have been deposited in the ArrayExpress database (www.ebi.ac.uk/arrayexpress) at the European Bioinformatics Institute under accession number E-MTAB-9091.

Preparation of samples for TCR libraries

Lymphocytes from Vβ5 mice were sorted as viable $CD8^+$ $CD4^-$ $TCRV\alpha2^+$ $CD62L^+$ $CD44^-$ (naive) or $CD44^+$ (AIMT). RNA was isolated using TRIzol (Thermo Fisher Scientific) followed by in-column DNase treatment using the RNA Clean & Concentrator Kit (Zymo Research). cDNA synthesis was performed using a TCR-specific primer (5′-TTGGCACCCG AGAATTCCACTGHHHHHACAHHHHHACAHHHHHCACATTGATTT GGGAGTC-3′) by using Maxima Reverse Transcriptase (Thermo Fisher Scientific) according to the manufacturer's instructions. The first round of PCR amplification was performed using primers 5′-CGTTCAGAGTTCT ACAGTCCGACGATCHHHHACHHHHACHHHNGCAGCCCATGGTAC CA GCAGTTCC-3′ and 5′-ACTGGAGTTCCTTGGCACCCGAGAATTC-3′, using KAPA HiFi HotStart ReadyMix (Kapa Biosystems) and the following conditions: 95°C for (5 min); 40 cycles at 98°C (20 s), 61°C (15 s), 72°C (15 s), and 72°C for (5 min). The resulting ∼440-bp-long PCR product was subjected to electrophoresis using an agarose gel and extracted using a Gel Extraction Kit (QIAGEN).

Following the first round of PCR, the TCRα copy number was quantified via quantitative PCR (LightCycler 480 II; Roche) and compared with a dilution series of OT-I TCRα cloned in MSCV vector. A total of 7.5×10^4 copies of the PCR product were then used for the second PCR amplification round using primers 5′-AATGATACGGCGACCACCGAGATCTACACG TTCAGAGTTCTACAGTCCGACGAT*C-3′ and 5′-CAAGCAGAAGAC GGCATACGAGATCGTGATGTGACTGGAGTTCCTTGGCACCC*G-3′. The polymerase was KAPA HiFi HotStart ReadyMix (2×) and the following conditions: 95°C (5 min); 40 cycles at 98°C (20 s), 62°C for (15 s), 72°C for (15 s), and 72°C for (5 min). The resulting ∼500-bp-long PCR product was subjected to electrophoresis in agarose gels and purified using Gel Extraction Kit (QIAGEN). The samples were mixed in equimolar ratios to obtain 30 μl of a final concentration of 10 nM and sequenced by Illumina MiSeq (v3 kit,; 300-bp paired-end reads) at the BIOCEV, Charles University, Vestec, Czech Republic.

Analysis of TCR repertoires

FastQC was used to assess read quality. Next, MIGEC version 1.2.9 (27) was used for quantification of clonotypes, and the resulting CDR3 sequence abundances in all samples were summarized to a clonotype abundance matrix. From this matrix, relative frequencies of CDR3 usage were computed. Clonotypes present in less than three samples were disregarded, and the clonotype abundance matrix was treated similar to RNA-sequencing count matrix,: DESeq2 was used to normalize for sequencing depth and RNA composition, and to test for differential clonotype abundance between AIMT and naive sample groups. Normalized abundances were used for principal component analysis (PCA).

For comparison of the diversity of TCR repertoires (CDR3 clonotypes), a Simpson Diversity Index was calculated using the function "diversity" from package "vegan" version 2.5-6 on R 4.0.2.

The sequence data has been deposited in the Sequence Read Archive and BioProject databases at National Center for Biotechnology Information. (https://www.ncbi.nlm.nih.gov/bioproject/PRJNA633838).

Feral mice

We analyzed feral mice *Mus musculus musculus* that were trapped in human houses or garden shelters in the region of Central Bohemia, Czech Republic. The mice used in this study were feral mice caught up to 1 mo prior to the analysis and 8- to 24-mo-old first generation (F1) offspring of the feral mice born in captivity. These mice were housed at the Department of Zoology, Faculty of Science, Charles University in Prague, Czech Republic. Mice were provided with food ad libitum and were kept under stable conditions in open cages (13/11 h, day:night, 23°C).

All animal procedures on feral mice were carried out in accordance with the law of the Czech Republic (paragraph 17, number 246/1992) and the local ethics committee of the Faculty of Science, Charles University in Prague, Czech Republic, and they were specifically approved for this study by accreditation number 13060/2014-MZE-17214.

Cohousing

Four SPF females were housed for 8 wk with one feral male per cage. The open cohousing cages were divided by a wire mesh with square openings (diameter was 1cm), allowing contacts of cohoused animals. Cohousing cages were supplied with fresh bedding at the beginning of the experiment and provided with water and food ad libitum.

The age of SPF females was 4- to 6-wk at the beginning of the cohousing experiment. The cohoused SPF females were matched with their littermates, which remained in the SPF facility and had the same food and the same bedding as the cohoused animals. We performed two experiments with slightly modified setups. For experiment A, during the 6-wk period of cohousing, the bedding was changed every 2 wk and the feral males were transferred into another cage. For experiment B, during the 6-wk period of cohousing, the bedding was not changed. Every 2 wk, the mice were transferred to the other side of the same cage to be exposed to the feces of the feral mice.

Collection of the samples for the microbiome analysis

A reference sample of saliva was collected from each mouse participating in the cohousing experiment before the start of experiment B. Throughout both experiments A and B, the saliva was collected from cohoused animals prior to the cohousing and after every second week of cohousing by gentle flushing with a pipette using 50 μl of the 0.9% NaCl solution. At the end of the experiment, the cohoused animals, as well as the non-cohoused controls, were sacrificed, and samples from duodenum, jejunum, ileum, cecum, and colon were collected for high-throughput 16S rRNA sequencing of the intestinal microbiota. At the end of each experiment, two cohoused Vβ5 animals and one cohoused feral male were sent for a thorough health status examination at the National Veterinary Institute in Prague. The results of this examination are available in health monitoring data submitted to Zenodo (https://zenodo.org/record/4298697#.YGxxu2RKhts).

Microbiota analysis by 16S rRNA sequencing

Metagenomic DNA from gut and saliva samples was extracted using the PowerSoil DNA Kit (MO BIO Laboratories, San Diego, CA). Barcoding was performed with previously published 16S rRNA primers Bact-0341-b-S-17 and S-D-Bact-0785-a-A-21 (28). Dual-indexed Nextera sequencing libraries were prepared using a previously published two-step PCR design (29). The first PCR was performed in 10 μl and consisted of 1× KAPA HiFi HotStart ReadyMix (Roche), each 16S rRNA primer at 0.2 μM and 3 μl DNA. PCR conditions were as follows: initial denaturation at 95°C for 3 min followed by 28 (for colon and cecum), 33 (for saliva), or 35 (ileum, duodenum,

Downloaded from http://www.jimmunol.org/ at Institute of Physiology ASCR on April 20, 2021

jejunum) cycles each of 95°C (30 s), 55°C (30 s), and 72°C (30 s) and a final extension at 72°C (5 min). The second PCR differed from the first PCR in the following parameters: it was performed in 20-μl volume; the concentration of each indexed primer was 1 μM; 1 μl (gut samples) or 6 μl (saliva) of the first PCR product were used as a template; and the number of PCR cycles was 12. Technical duplicates were prepared to account for noise due to PCR and sequencing stochasticity. PCR products were pooled equimolarly, size-selected with Pippin Prep (Sage Science, Beverly, MA) at 520–750 bp and sequenced using MiSeq (Illumina, San Diego, CA) and v3 chemistry (i.e., 2 × 300-bp paired-end reads). Sequencing data were archived in European Nucleotide Archive under project accession PRJEB38301.

Samples were demultiplexed and primers were trimmed by skewer software (30). Using DADA2 (31), we filtered out low-quality sequences (expected number of errors per read >1), denoised the quality-filtered fastq files, and constructed an abundance matrix representing reads counts for individual haplotypes in each sample. Using UCHIME (32) and the gold.fna database, we identified chimeric sequences and removed them from the abundance matrix. Taxonomic assignation of haplotypes was conducted by the Ribosomal Database Project classifier (80% confidence threshold) (33) and the SILVA reference database v132 (34).

The effect of cohousing on α-diversity (based on Shannon diversity indices) was tested using a linear mixed-effect model, considering individual identity as a random effect and the effect of treatment level (cohoused versus non-cohoused), gut section, and their interactions as explanatory variables. The effect of cohousing on microbiota composition was assessed by permutation tests, in which the observed difference in composition (i.e., Bray–Curtis similarities) between cohoused laboratory versus wild individuals and non-cohoused laboratory versus wild individuals was compared with permuted average differences, where belonging to the cohoused versus non-cohoused laboratory group was randomized. Individual haplotypes whose relative abundances were affected by cohousing were identified by the DESeq2 package (24).

Results

The frequency of AIMT cells increases in germ-free mice during aging

It has been shown that the percentage of AIMT cells increases upon aging (35–39). However, these studies have used conventional SPF mice, and thus the role of microbial Ags in this process cannot be excluded. Moreover, previous studies analyzed only B6 mice but not BALB mice that show substantial differences in the site of origin and cytokine dependency of AIMT cells (5, 3). For this reason, we compared the $CD8^+$ T cell compartment in young and aged germ-free B6 and BALB mice. We observed that the frequency of peripheral $CD44^+$ $CD49d^-$ AIMT cells increases in both strains upon aging (Fig. 1A, 1B; Supplemental Fig. 1A, 1B), suggesting a common homeostatic mechanism of age-dependent induction of AIMT cells.

Peripherally derived AIMT cells express high levels of CD122

AIMT cells from B6 mice depend on IL-15 and express high levels of CD122 (IL-2RB), a subunit of the IL-15 receptor (5, 7, 16). We observed that AIMT cells from young germ-free B6 mice express higher levels of CD122 than those from young BALB mice (Fig. 1C, 1D; Supplemental Fig. 1C, 1D). Interestingly, a population of $CD122^{HIGH}$ AIMT cells appears in aged germ-free BALB mice, whereas no difference in CD122 expression was found between AIMT cells from germ-free young and aged B6 mice (Fig. 1C, 1D). We observed that $CD122^{HIGH}$ AIMT cells show slightly stronger homeostatic proliferation than $CD122^{LOW}$ AIMT cells in aged but not in young BALB mice (Fig. 1E, 1F), which probably contributes to their accumulation in aged mice.

$CD122^{HIGH}$ AIMT cells in B6 mice are generated in the periphery via IL-15 and homeostatic TCR signaling (6, 17). These cells are more frequent in aged mice, probably because the thymic output is low and the lymphopenic environment augments AIMT cells formation. In contrast, $CD122^{LOW}$AIMT cells are generated in the thymus of young BALB mice via IL-4 (3). We hypothesized that, during aging of BALB mice, the thymic regress impairs de novo formation of $CD122^{LOW}$ AIMT cells, leading to the lymphopenia-induced generation of proliferative $CD122^{HIGH}$ AIMT cells in the periphery. To elucidate whether CD122 expression could discriminate between thymic (innate memory) and peripheral AIMT cells (virtual memory) in BALB mice, we employed two models for lymphopenia-induced AIMT cells formation.

The first lymphopenic model was sublethal irradiation of mice. Irradiation reduces the number of T cells, which leads to homeostatic proliferation and AIMT formation of the surviving T cells in the periphery (1). As expected, irradiation increased the frequency of AIMT cells in B6 and BALB mice (Fig. 2A, 2B). Irradiation-induced AIMT cells showed significantly higher CD122 expression than control AIMT cells in BALB but not in B6 mice (Fig. 2C, 2D). This result is in close agreement with the hypothesis that CD122 expression is a marker of peripherally induced AIMT cells in both strains.

The second model was TCR transgenic DO11.10 Rag^+ BALB mice. Most of T cells in these mice are monoclonal $CD4^+$ T cells specific to $I\text{-}A^d\text{-}OVA_{323\text{-}339}$ (40). However, rare T cells expressing endogenous TCRα differentiate into $CD8^+$ T cells. Thymic AIMT cells should be substantially reduced in these mice because of the absence of IL-4–producing thymic iNKT cells that are crucial for the formation of thymic AIMT cells (3). In addition, this mouse is lymphopenic in the $CD8^+$ T cell compartment, which should promote the formation of AIMT cells in the periphery.

DO11.10 mice showed comparable frequency of AIMT cells with polyclonal BALB mice. The frequency of AIMT $CD8^+$ T cells during aging increased (Fig. 2E, 2F), indicating that the age-dependent increase in the AIMT cell compartment does not depend on the presence of iNKT cells. The expression of CD122 was higher in AIMT cells from DO11.10 mice than in AIMT cells from polyclonal BALB mice (Fig. 2G), which is consistent with the hypothesis that $CD122^{HIGH}$ AIMT cells are formed in the periphery. When we transferred naive polyclonal $CD8^+$ T cells into the DO11.10 mice, we observed the formation of AIMT cells, which was coupled with their homeostatic proliferation (Fig. 2H, 2I).

Overall, these data indicate that CD122 expression differs between peripherally induced virtual memory AIMT cells (both in B6 and BALB mice) and thymus-derived innate memory AIMT cells of BALB mice.

The site of origin and aging fine-tune the gene expression profile of AIMT cells

The AIMT cell compartment is heterogeneous. As mentioned above, AIMT cells are formed in different organs (thymus or peripheral lymphoid organs) and have distinct cytokine dependencies (IL-15 versus IL-4) in different strains. Moreover, aging might change the gene expression programs of AIMT cells (36–38). We addressed differences between particular AIMT cell populations by high-throughput RNA sequencing using sorted naive and AIMT cells from young B6 and BALB mice, irradiation-induced AIMT cells from B6 and BALB mice, AIMT cells from aged B6 mice, and $CD122^{LOW}$ and $CD122^{HIGH}$ AIMT cells from aged BALB mice (Supplemental Fig. 1E–I).

As expected, the major source of the variability among these samples was the different genetic background of B6 and BALB mice (Supplemental Fig. 2A). We normalized the gene expression data for the differences between the strains by fitting the data with a linear model using the strain identity as one of the explanatory variables (Fig. 3A). The expression of *Il2rb* (CD122) and *Itga4* (CD49d) in the sorted populations corresponded to the sorting strategy (Fig. 3B) and the previous characterization of AIMT cells from both mouse strains (Fig. 1A–D).

We assumed that naive and irradiation-induced AIMT cells represent two relatively uniform cell types present in both strains, and we

Downloaded from http://www.jimmunol.org/ at Institute of Physiology ASCR on April 20, 2021

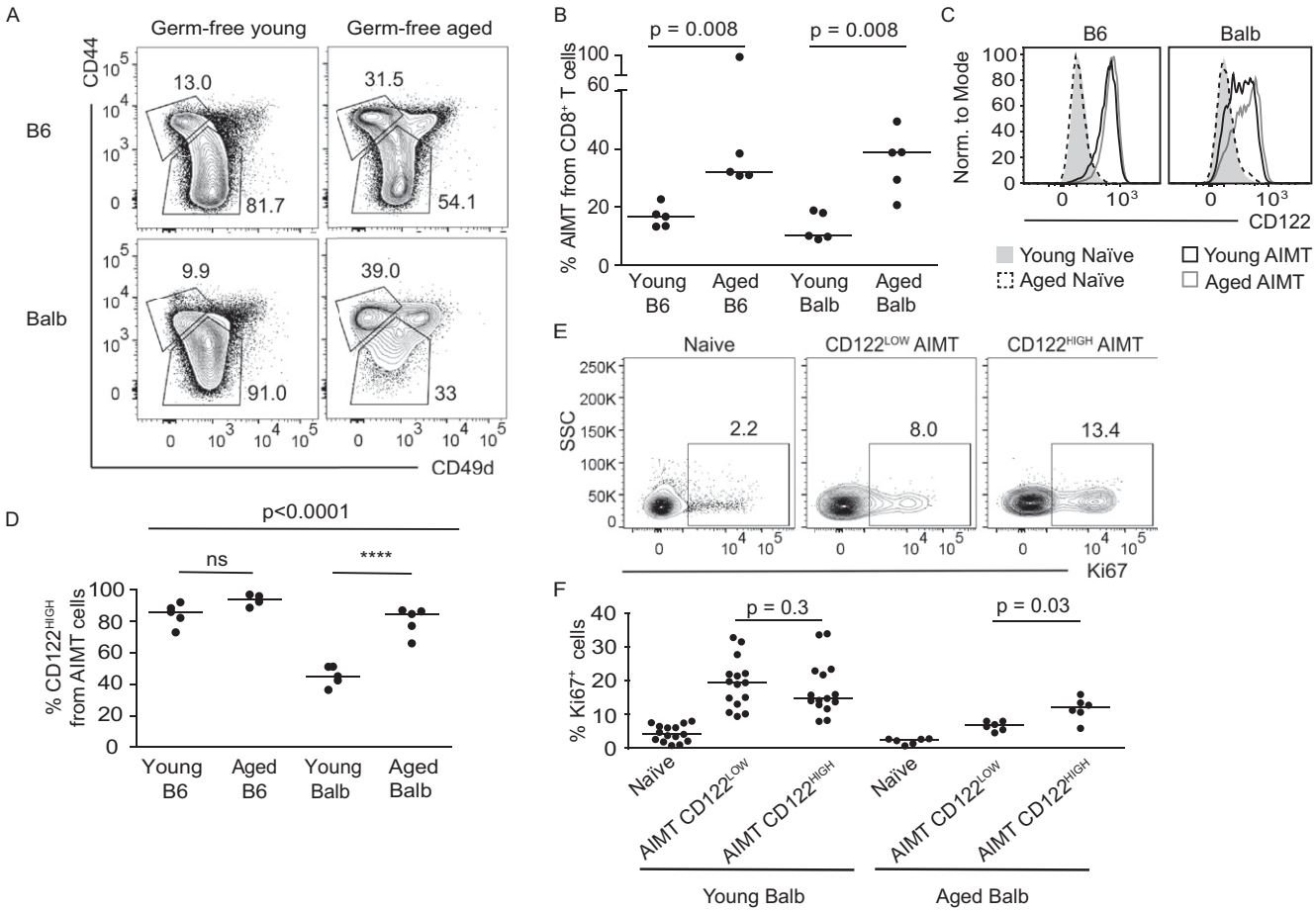

FIGURE 1. AIMT cells increase during aging in germ-free mice. (**A**–**D**) T cells from spleens of germ-free young (5–12 wk) or aged (55–75 wk) mice were stained for viability, TCRβ, CD8α, CD44, CD49d, and CD122 and analyzed by flow cytometry. (A) A representative staining of $CD8^+$ T cells for CD44 and CD49d. Gates for naive ($CD44^-$) and AIMT ($CD44^+$ $CD49d^-$) cells are shown. One representative experiment out of two in total is shown. (B) Quantification of the percentage of $CD44^+$ $CD49d^-$ AIMT cells among $CD8^+$ T cells. $n = 5$ mice from two to five independent experiments. Median is shown. The statistical significance was tested using two-tailed Mann–Whitney U test. (C) Histograms of CD122 expression in $CD44^-$ naive and $CD44^+$ $CD49d^-$ AIMT $CD8^+$ cells from indicated mice. One representative experiment out of two in total is shown. (D) Quantification of $CD122^{HIGH}$ cells among $CD8^+$ AIMT cells. Median is shown. The statistical significance was tested using ANOVA with Bonferroni multiple comparison posttests of indicated pairs. A p value <0.0001 was significant. **** $p \leq 0.0001$. (**E**–**F**) Splenocytes from young and aged SPF BALB mice were fixed and stained for CD8α, CD44, CD49d, CD122, and Ki67. (E) Ki67 expression in naive, $CD122^{HIGH}$ and $CD122^{LOW}$ AIMT cells of aged mice. A representative mouse out of six in total is shown. (F) Percentage of $Ki67^+$ cells is shown. $n = 6$ (aged) or 15 (naive) mice in six or three independent experiments, respectively. The statistical significance was tested using two-tailed Wilcoxon matched-pairs signed-rank test. Median is shown.

used them as controls for evaluating our data normalization. The PCA of the adjusted data revealed that naive cells and irradiation-induced AIMT cells from both strains clustered together, confirming the reliability of our adjusted data (Fig. 3A). We obtained very similar results when performing the PCA using data without strain-specific normalization but with the exclusion of significantly differentially expressed genes between the strains (Supplemental Fig. 2B).

The AIMT cells from aged mice showed moderate differences in their gene expression patterns in comparison with AIMT cells from young animals (Fig. 3A). We identified 36 genes upregulated in AIMT cells from aged mice versus young mice in both strains (Supplemental Fig. 2C). Twenty-four of these transcripts were at least 4-fold enriched in AIMT cells from aged B6 mice in comparison with young mice in the previous study by Quinn et al. (36). Interestingly, we did not identify a single gene significantly upregulated in AIMT cells from young mice versus aged mice in both strains.

Young AIMT cells from both strains showed comparable global gene expression signature. The gene expression similarity between these populations was revealed as the proximity of young AIMT cells from both strains in the PCA plots (Fig. 3A, Supplemental Fig. 2B) as well as a correlation of AIMT/naive cell fold changes for individual genes plotted as B6 versus BALB without using any correction for the strain-dependent differences (Fig. 3C). Despite the similarity of the gene expression patterns, we could identify one gene significantly upregulated, and 25 genes significantly downregulated in young BALB AIMT cells versus B6 AIMT cells (Fig. 3D), suggesting that these genes might distinguish thymic innate memory and peripheral virtual memory subsets of AIMT cells.

We observed that the genes upregulated in AIMT cells from young B6 versus young BALB mice are significantly enriched in aged $CD122^{HIGH}$ AIMT cells versus aged $CD122^{LOW}$ AIMT cells from aged BALB mice (Fig. 3D, 3E), supporting the hypothesis that high CD122 levels predict the peripheral origin of AIMT cells, irrespective of the strain.

It has been proposed that T-bet (*Tbx21*) and NKG2D (*Klrk1*) are expressed in peripheral but not in thymic AIMT cells (2). Moreover, a small group of genes potentially involved in bystander cytotoxicity (*Gzmb*, *Il12rb2*, *Il18r1*, *Il18rap*, *Stat4*) were shown to be upregulated in peripheral AIMT cells (2, 6). All of these genes but *Gzmb*

Downloaded from http://www.jimmunol.org/ at Institute of Physiology ASCR on April 20, 2021

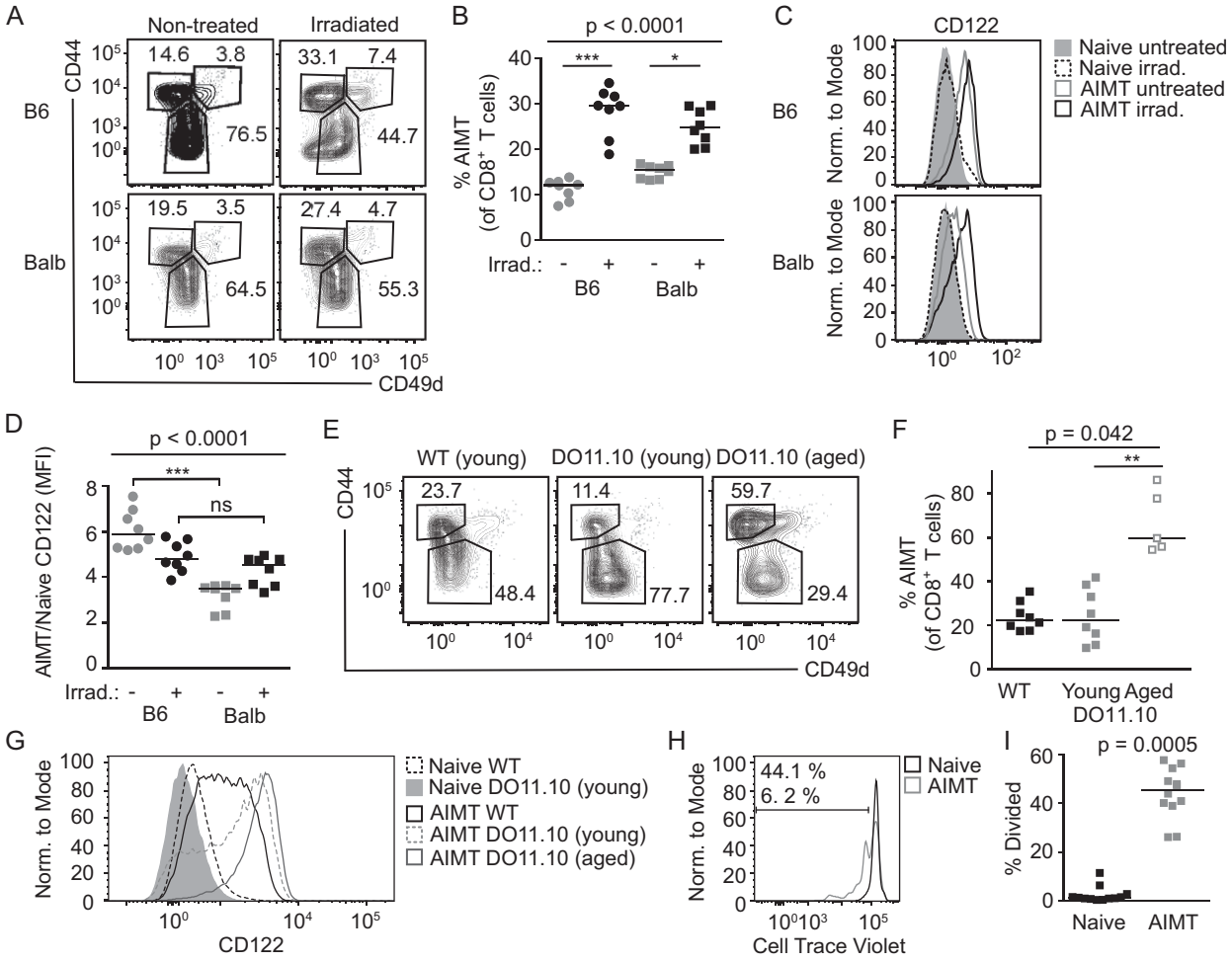

FIGURE 2. Lymphopenia induces CD122^{HIGH} AIMT cells in BALB mice. (**A–D**) Five- to eight-wk-old SPF B6 and BALB mice were sublethally irradiated or not. 16 d later, the mice were sacrificed and the splenocytes were stained for TCRβ, CD8α, CD44, CD49d, and CD122 and analyzed by flow cytometry. $n = 8$ mice per group in four independent experiments. (A) One representative experiment out of total is shown. (B) Quantification of the frequency of AIMT cells. Median is shown. The statistical significance was tested using Kruskal–Wallis test with Dunn multiple comparisons posttests. *** $p < 0.001$, * $p < 0.05$. (C) Expression of CD122 in naive and AIMT cells in untreated and irradiated B6 and BALB mice. (D) Quantification of CD122 expression in AIMT cells normalized to the expression on naive T cells. Median is shown. The statistical significance was tested using Kruskal–Wallis test with Dunn multiple comparisons posttests. A p value >0.05 was ns. *** $p < 0.001$. (**E–G**) Splenocytes from young (5–14 wk) BALB and young or aged (52–73 wk) DO11.10 mice were stained for TCRβ, CD8α, CD44, CD49d, and CD122 and analyzed by flow cytometry. $n = 8$ or 5 (aged DO11.10) mice in four to five independent experiments. (E) Representative experiments showing CD44 and CD49d staining of CD8$^+$ T cells. (F) Quantification of the frequency of AIMT cells among CD8$^+$ T cells. Median is shown. The statistical significance was tested using Kruskal–Wallis test with Dunn multiple comparisons posttests. ** $p < 0.01$. (G) Expression of CD122 in young BALB and young and aged DO11.10 naive and AIMT CD8$^+$ T cells. (**H** and **I**) CellTrace Violet–loaded naive CD8α$^+$ CD44$^-$ CD49d^{LOW} T cells isolated from lymph nodes and spleen from BALB mice were adoptively transferred into DO11.10 mice. Seven days later, the lymph nodes of the recipient mice were analyzed by flow cytometry. CellTrace Violet signal in cells that stayed naive (CD44$^-$ CD49d^{LOW}) and cells converted into AIMT (CD44$^+$ CD49d$^-$) is shown. $n = 12$ host mice in three independent experiments. (H) The CellTrace Violet dye dilution in naive (CD44$^-$) and AIMT (CD44$^+$ CD49d$^-$) adoptively transferred cells (live TCRβ$^+$ CD8$^+$ TCRVβ8.1/8.2$^-$) is shown. One representative experiment out of three in total is shown. (I) The percentage of adoptively transferred naive or AIMT cells that underwent at least one cycle of division is shown. Median is shown. The statistical significance was tested using Wilcoxon matched-pairs signed-rank test.

were enriched in young AIMT cells over naive T cells in our data (Fig. 3F). Four genes (*Tbet*, *Klrk1*, *Il18r1*, *Il18rap*) showed higher expression in AIMT cells of the proposed peripheral origin (AIMT cells from young and aged B6 and CD122^{HIGH} AIMT cells from aged BALB mice) than in the corresponding AIMT cells of the proposed thymic origin (AIMT cells from young BALB and CD122^{LOW} AIMT cells from aged BALB mice) (Fig. 3F).

Flow cytometry confirmed higher expression of IL-18R in AIMT cells from B6 than from BALB mice (Fig. 3G, Supplemental Fig. 2D). Moreover, IL-18R was preferentially expressed in CD122^{HIGH} AIMT cells (Supplemental Fig. 2E). Accordingly, AIMT cells from B6 mice were more efficient in producing IFN-γ after stimulation with IL-12/IL-18 than AIMT cells from BALB mice, whereas the responses of these cells to PMA and ionomycin were comparable (Fig. 3H, Supplemental Fig. 2F).

Overall, these data revealed a stable gene expression program in AIMT cells that is fine-tuned by the age and genetic background. The most notable variation among AIMT cells is the differential expression of genes encoding proinflammatory receptors based on the site of their origin. Peripheral AIMT cells express higher levels of CD122 (a receptor for IL-2 and IL-15), IL-18R, and activating NKG2D receptor than thymic AIMT cells. This expression pattern predisposes peripheral AIMT cells for efficient bystander immune protection.

Downloaded from http://www.jimmunol.org/ at Institute of Physiology ASCR on April 20, 2021

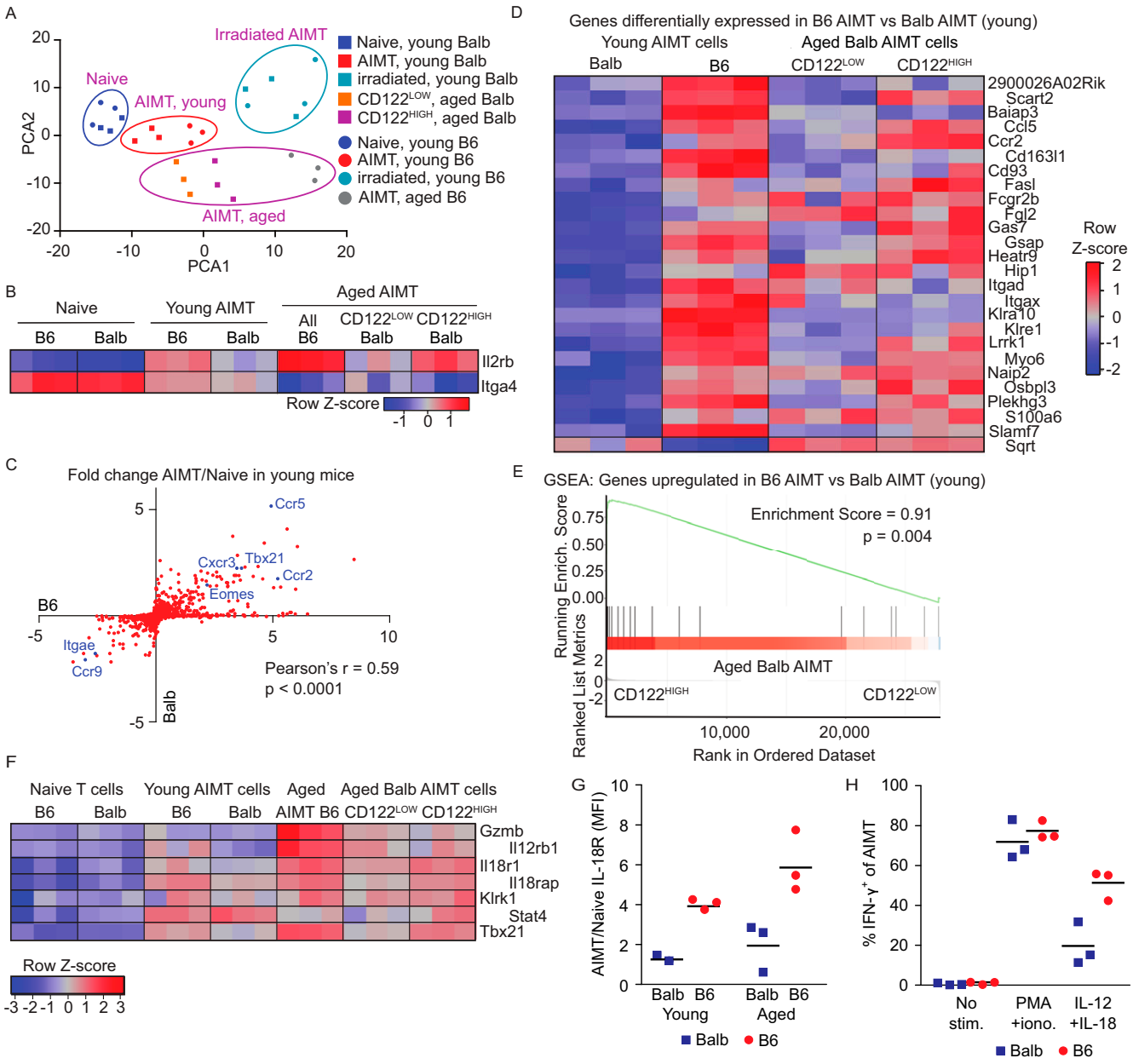

FIGURE 3. Similar gene expression profiles of thymic and peripheral AIMT cells. (**A–E**) Naive ($CD44^-$) and/or AIMT ($CD44^+$ $CD49d^-$) $CD8^+$ T cells were sorted from lymph nodes and spleens from young (5–12 wk) untreated or young irradiated (4 Gy, 3 wk) B6 and BALB or aged B6 mice (76 wk). $CD122^{HIGH}$ and $CD122^{LOW}$ AIMT cells were sorted from lymph nodes and spleens from aged BALB mice (54–55 wk). The transcriptome of these populations was analyzed by RNA sequencing. (A) PCA analysis of the gene expression profiles of the individual samples normalized to avoid the strain-specific differences (top 500 variable genes). (B) Relative expression (*z*-score) of Il2rb (CD122) and Itga4 (CD49d) in individual samples using normalization for strain-specific differences. (C) Ratios of transcript levels in AIMT cells to naive cells (young mice) were calculated for each gene and plotted as $\log_2$ for B6 and BALB strains. Selected genes are indicated. The correlation was calculated using Pearson correlation coefficient. (D) Relative expression (*z*-score) of genes showing significantly different expression between AIMT cells from young B6 and BALB mice (after the normalization for strain-specific differences) in AIMT cells from B6 and BALB mice and in $CD122^{HIGH}$ and $CD122^{LOW}$ AIMT cells from aged BALB mice. (E) The gene set enrichment analysis (GSEA) of genes with significantly higher expression in B6 than in BALB mice [shown in (D)] in $CD122^{HIGH}$ versus $CD122^{LOW}$ AIMT cells from aged BALB mice. (**F**) Relative expression (*z*-score) of selected genes involved in bystander cytotoxicity between AIMT cells from young B6 and BALB mice (after the normalization for strain-specific differences) in AIMT cells from B6 and BALB mice and in $CD122^{HIGH}$ and $CD122^{LOW}$ AIMT cells from aged BALB mice. (**G**) Expression of IL-18R on the surface of AIMT cells from the lymph nodes of young and aged BALB and B6 mice measured by flow cytometry. Geometric mean fluorescent intensity (MFI) was normalized to naive cells in the same sample. Mean is shown. $n = 3$ independent experiments. (**H**) Production of IFN-γ by AIMT cells (gated as $CD8\alpha^+$ $CD44^+$ $CD49d^+$) from young adult B6 or BALB mice was measured by flow cytometry. Lymph node cells were stimulated with PMA plus ionomycin or with IL-12 and IL-18 or left unstimulated for 8 h and analyzed by flow cytometry. $n = 3$ independent experiments.

Young and aged AIMT cells represent identical TCR clonotypes

The frequency of murine AIMT cells changes over time. It peaks around 3 wk of age (41), and it increases again as the mouse ages (35). For this reason, it is unclear whether AIMT cells in young and aged animals have a different clonal origin (42). To address this question, we analyzed TCR sequences of

Downloaded from http://www.jimmunol.org/ at Institute of Physiology ASCR on April 20, 2021

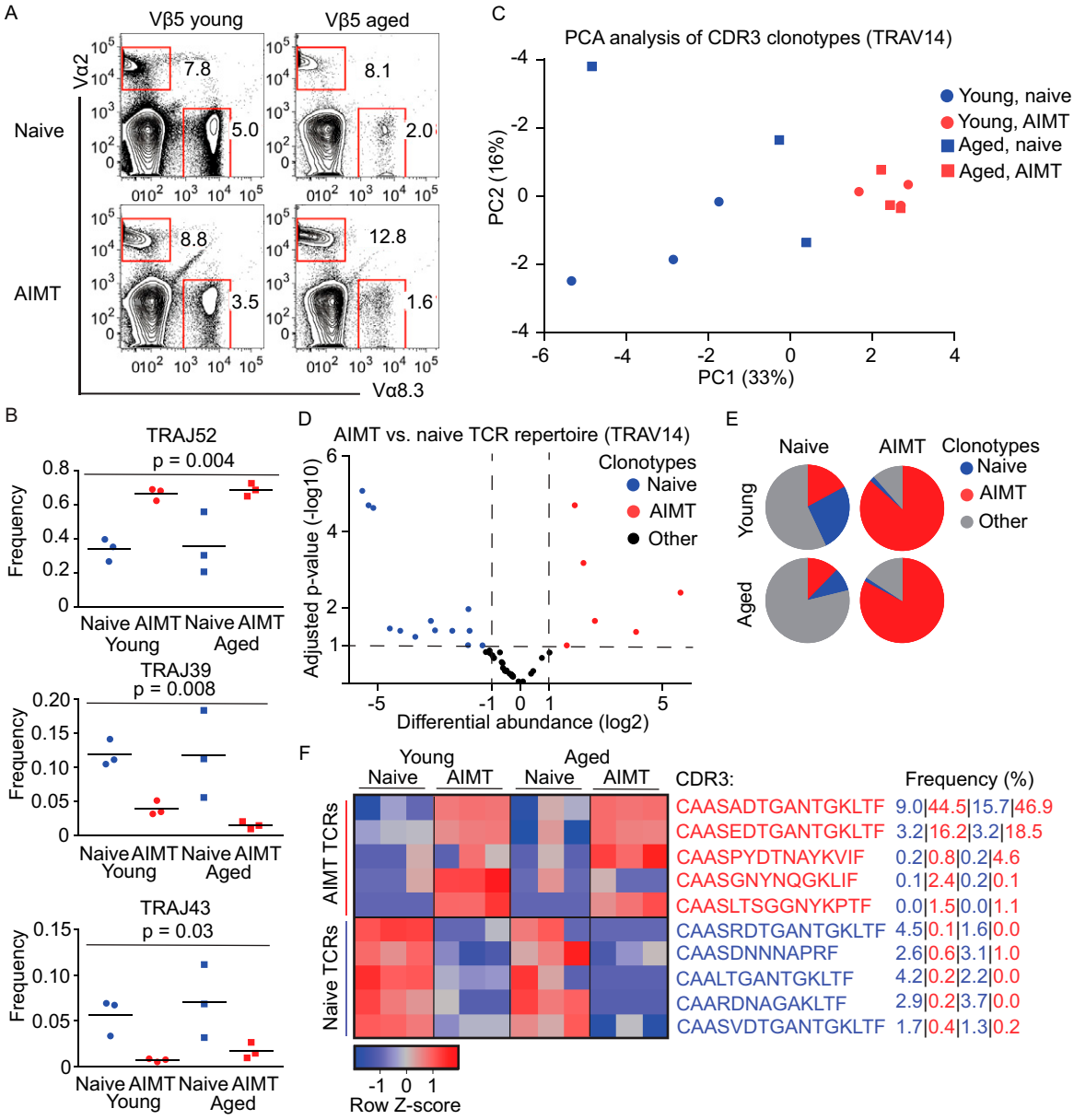

FIGURE 4. AIMT cells in young and aged mice represent identical clones. (**A–F**) Lymph node cells from young (7–12 wk) and aged (65–77 wk) Vβ5 mice were enriched for $CD8^+$ T cells by magnetic beads and stained for CD8, CD44, CD62L, CD49d, TCRVα2, and TCRVα8.3. Two to three mice were pooled for each sample. $n = 3$ independent experiments. (A) The percentage of $TCRV\alpha2^+$ and $TCRV\alpha8.3^+$ among AIMT and naive $CD8^+$ T cells is shown. (B–F) AIMT ($CD44^+$ $CD62L^+$) and naive ($CD44^-$ $CD62L^+$) $TCRV\alpha2^+$ $CD8^+$ T cells were FACS sorted. Library of TCR sequences was generated from isolated RNA using a two-step PCR and analyzed by deep sequencing. (B) Frequency of TRAJ52, TRAJ39, and TRAJ43 usage among the analyzed samples. Mean is shown. The statistical significance was tested using one-way repeated measures ANOVA. (C) PCA analysis of the TCR clonotype (based on CDR3 amino acid sequence) usage in the individual samples. Only clonotypes detected in at least three samples were included in the analysis. (D) A volcano plot showing $\log_2$ differential usage between naive and AIMT cells (both young and aged) and adjusted p value for each individual TCR clonotype present at least in three samples. AIMT, naive (2-fold difference in usage, adjusted $p < 0.01$) and "neutral" (nonsignificant) clonotypes are indicated in red, blue, and gray, respectively. (E) Pie charts showing the abundance of the AIMT, naive, and neutral clonotypes in the T cell repertoires of young and aged Vβ5 mice. (F) Relative usage (z-score) of five most abundant AIMT and five most abundant naive clonotypes in the indicated samples. The average frequency of each clone in young naive, young AIMT, aged naive, and aged AIMT repertoires is indicated on the right.

naive and AIMT cells in young and aged mice. To overcome the problem with TCRα and TCRβ pairing, we analyzed TCR α-chains in a Vβ5 mouse that has a fixed TCRβ from the OT-I TCR.

Because central memory $CD8^+$ $CD44^+$ $CD62L^+$ T cells in Vβ5 mice do not express CD49d (Supplemental Fig. 3A), we gated AIMT cells in Vβ5 mice as $CD44^+$ $CD62L^+$ double-positive. The frequency of AIMT cells in Vβ5 mice recapitulates WT mice, including the increase in the frequency of AIMT cells upon aging (Supplemental Fig. 3B).

First, we quantified the usage of TRAV14 (corresponding to Vα2 epitope) and TRAV12 (corresponding to Vα8.3) by staining with specific Abs. In line with our previous data (17), we observed a higher Vα2/Vα8.3 ratio in AIMT cells than in naive T cells of young mice (Fig. 4A, Supplemental Fig. 3C). Interestingly, the Vα2/Vα8.3 ratio in naive cells was higher in aged mice than in

Downloaded from http://www.jimmunol.org/ at Institute of Physiology ASCR on April 20, 2021

young mice (Supplemental Fig. 3C). The highest Vα2/Vα8.3 ratio was observed in the AIMT compartment in aged mice. Because $V\alpha2^+$ T cells are, on average, more self-reactive than $V\alpha8.3^+$ T cells in Vβ5 mice (17), our data suggest that the $CD8^+$ T cell compartment in aged mice is enriched for self-reactive T cells and that AIMT cells are generally more self-reactive than naive cells in young as well as in aged mice.

In the next step, we analyzed TCRs from $V\alpha2^+$ T cells in greater detail using high-throughput sequencing. Naive and AIMT cells showed differential usage of TRAJ segments, indicating that they are formed from different T cell clonotypes (Fig. 4B, Supplemental Fig. 3D), which is in line with previous results (8, 17). Interestingly, we did not see any differences in the TRAJ usage between young and aged mice (Fig. 4B, Supplemental Fig. 3D). The second step of our analysis was the comparison of individual clonotypes using CDR3 amino acid sequences. The PCA analysis separated a cluster of AIMT cells (both young and aged mice) from naive T cells (Fig. 4C). The comparison of the usage of individual clonotypes by naive and AIMT cells showed that some clonotypes are enriched in the naive compartment and some clonotypes are significantly enriched in AIMT cells (Fig. 4D). The AIMT cell repertoire in young and aged mice is constituted predominantly from a small number of AIMT cell–enriched clonotypes. In contrast, the naive repertoire is more diverse and contains naive-enriched as well as AIMT-enriched clones (Fig. 4E). The usage of the dominant clonotypes differ in naive and AIMT subsets but not so much between the corresponding subsets from young and aged mice (Fig. 4F). Accordingly, the diversity of the TCR repertoire is relatively high in naive T cells and relatively low in AIMT T cells, irrespective of the age of the animals (Supplemental Fig. 3E). Overall, these data showed that AIMT cells from young and aged mice have the same clonal origin, although it is possible that some minor clonotypes are lost from the AIMT repertoire during aging, as indicated by the reduction of TCR Vα8.3 clonotypes.

AIMT cells in feral mice

It has been suggested that the exposure to environmental Ags in feral and "pet shop" mice has a substantial role in shaping the $CD8^+$ T cell compartment (18). To address the possibility that the occurrence of AIMT cells might be an artifact of specific hygienic conditions in germ-free and SPF facilities, we analyzed mice with natural microbial colonization. First, bred feral mice in the animal facility and analyzed F1 offspring born in captivity. Interestingly, we observed that AIMT cells are relatively frequent in these mice (Fig. 5A, 5C). The expression of CD122 was variable between individual animals, suggesting variable peripheral or thymic origin of these cells, likely based on the environmental or genetic factors (Fig 5A).

In the next step, we analyzed feral mice trapped in garden shelters and human houses. These mice are supposed to have even richer antigenic exposure history that the F1 feral mice born in captivity. We observed that these mice contain a large population of $CD8^+$ $CD44^+$ $CD49d^-$ T cells, corresponding to AIMT cells (Fig. 5B, 5C). The expression of CD122 in these AIMT cells largely varied among individual animals (Fig. 5B). Overall, these data suggested that the population of AIMT cells exists in feral mice. Interestingly, the percentage of AIMT cells was higher in feral mice than in F1 offspring of feral mice kept in captivity (Fig. 5C). This indicated that exposure to environmental Ags might increase the size of the AIMT cell compartment, as was recently shown for helminth infections (43, 44). The relative size of the AIMT cell compartment correlated with the frequency of $CD122^{HIGH}$ cells among them in feral mice (Fig. 5D). This indicates that environmental factors inducing AIMT cells preferentially induce $CD122^{HIGH}$ peripheral virtual memory T cells. This correlation was not observed in F1 offspring of feral mice, indicating the major role of genetic background (Fig. 5E).

Cohousing of laboratory and feral mice has minimal effects on the $CD8^+$ T cell compartment

To observe how the AIMT cell compartment and other $CD8^+$ T cell subsets change upon exposure to environmental Ags in laboratory mice, we cohoused B6 WT mice and transgenic Vβ5 mice with feral mice or F1 offspring of feral mice for 6 wk. Surprisingly, the cohousing had no significant effect on the proportions of the major $CD8^+$ T cell subsets (i.e., naive, AIMT, and Ag-experienced [AgE] cells) in B6 and Vβ5 mice (Fig. 5F–H). The only observed difference between cohoused and control laboratory strains was a slightly higher percentage of $CX3CR1^+$ $CD44^+$ $CD49d^+$ AgE cells in the spleen and mesenteric lymph nodes of the cohoused animals of the SPF origin (Fig. 5G).

We observed that the enrichment of the AIMT cell compartment in $V\alpha2^+$ T cells was preserved in the cohoused animals (Fig. 5I), suggesting that the cohousing did not substantially alter the composition of the repertoire of the AIMT cell compartment. Overall, our data indicate that AIMT cells are a naturally occurring $CD8^+$ T cell subset in laboratory mouse strains as well as in feral mice.

Limited effects of cohousing on the microbial colonization

Because we observed a surprisingly small effect of the cohousing of laboratory strains with feral mice or F1 offspring of feral mice on their $CD8^+$ T cell compartment, we examined the colonization of the feral and cohoused animals with microbes and viruses. A detailed health examination of a limited number of animals detected *Helicobacter*, *Pasteurella*, murine CMV, and endoparasites but no other pathogenic agents in the feral mice (see https://zenodo.org/record/4298697#.YGxxu2RKhts). Of these pathogens, only *Helicobacter* and endoparasites were transmitted to the cohoused animals in at least one case out of four tested cohoused mice. This was in line with the fact that none of the cohoused mice died before the end of the experiment, including Vβ5 mice, which are most likely immunocompromised because of the limited TCR repertoire.

Subsequently, we addressed the effects of cohousing on bacterial colonization. We performed 16S rRNA sequence analysis of the composition of the microbial community in the gut and salivary glands of cohoused animals. The overall microbial diversity in the intestine of cohoused laboratory strains was not affected, except for the ileum, where the diversity increased (Supplemental Fig. 4A). Interestingly, microbial diversity decreased in the colon of feral mice upon cohousing (Supplemental Fig. 4A). As expected, the microbial composition of the intestine of the laboratory strains converged to the feral mice upon cohousing (Fig. 6A, Supplemental Fig. 4B). The most notable effect of the cohousing was the abundance of *Campylobacteria* (a taxon including *Helicobacter*) in the colon and cecum of the cohoused mice, whereas this group of bacteria was not present in non-cohoused laboratory mice (Fig. 6B, Supplemental Fig. 4C). Two different *Helicobacter* taxons (Campylobacterales) and *Alistipes* (Bacteroidia) were detected in the colon and cecum of some of the cohoused but not SPF mice (Fig. 6C). In contrast, three taxonomic units from Clostridiales, *Roseburia*, and *Ruminococcus* taxons were depleted in colon, cecum, and duodenum of the cohoused mice (Supplemental Fig. 4D).

The salivary microbiome of the laboratory strains did not converge to feral mice, but rather the microbiome of the feral mice converged to the microbiome of SPF laboratory strains during the cohousing (Supplemental Fig. 4E). However, cohousing led to a dramatic increase in Bacteriodia taxon in saliva of laboratory strains (Fig. 6D, Supplemental Fig. 4F). Moreover, the abundance of Clostridia and Deltaproteobacteria was detected in some individuals

Downloaded from http://www.jimmunol.org/ at Institute of Physiology ASCR on April 20, 2021

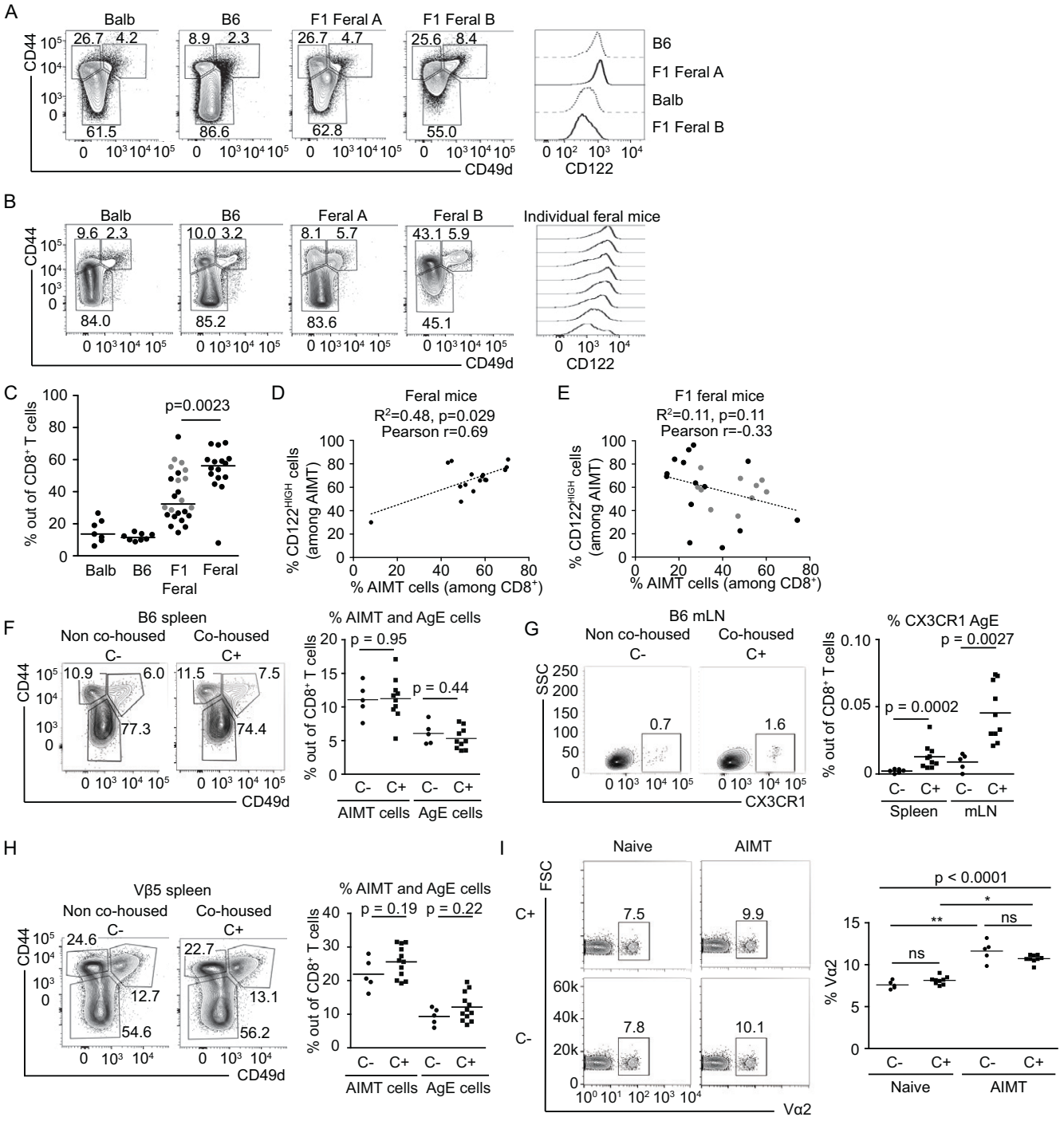

FIGURE 5. AIMT cells are present in feral mice and in laboratory mice cohoused with feral mice. (**A**–**C**) Spleens of laboratory B6 and BALB strains and F1 offspring of feral mice (A and C) or feral mice (B and C) were isolated, fixed with formaldehyde, and stained for CD8, CD44, CD49d, and CD122 and analyzed by flow cytometry. Percentage of naive ($CD44^-$), AIMT ($CD44^+$ $CD49d^-$), and AgE ($CD44^+$ $CD49d^+$) cells among $CD8^+$ T cells and CD122 expression in AIMT cells is shown. (C) Percentages of AIMT cells among $CD8^+$ T cells in B6 or BALB mice, F1 offspring of feral mice (young adult 5- to 8-wk-old, gray marks or aged 8- to 24-mo-old, black marks) or feral mice. BALB: $n = 6$ mice/six independent experiments; B6: $n = 7{:}7$; F1 offspring of feral mice: $n = 14{:}5$, feral mice $n = 16{:}2$. Median is shown. The statistical significance was tested using two-tailed Mann–Whitney U test. (**D** and **E**) The percentages of AIMT cells among $CD8^+$ T cells versus $CD122^{HIGH}$ cells among AIMT cells were plotted for each individual mouse for feral mice (D) or for F1 offspring (young adult 5- to 8-wk old, gray marks or aged 8- to 24-mo-old, black marks) of feral mice (E). The linear regression line and p value (calculated by F test) for a deviation of the regression line from a horizontal line is shown. Moreover, Pearson correlation coefficient is shown. (**F**–**I**) B6 or Vβ5 mice were or were not cohoused (C+ and C−, respectively) with feral mice or F1 offspring of feral mice for 6 wk, and their splenocytes were analyzed by flow cytometry. For B6 mice, $n = 5$ (C−) or 10 (C+) mice in two independent experiments. For Vβ5 mice, $n = 5$ (C−) or 12 (C+) mice in two independent experiments, if not indicated otherwise. (F) Percentages of naive ($CD44^-$), AIMT ($CD44^+$ $CD49d^-$), and AgE ($CD44^+$ $CD49d^+$) cells among $CD8^+$ T cells in cohoused (C+) or non-cohoused (C−) B6 mice. A representative experiment (left) and the quantification (right) are shown. Mean is shown. Statistical significance was calculated using two-tailed Mann–Whitney U test. (G) Percentages of $CX3CR1^+$ AgE cells among $CD8^+$ T cells from mesenteric lymph nodes (mLN) or spleens of cohoused (C+) or non-cohoused (C−) B6 mice. A representative experiment (left) and the quantification (right) are shown. Statistical significance was calculated using two-tailed Mann–Whitney U test. (H) Percentages of naive ($CD44^-$), AIMT ($CD44^+$ $CD49d^-$), and AgE ($CD44^+$ $CD49d^+$) cells among $CD8^+$ T cells in cohoused (C+) or non-cohoused (C−) Vβ5 mice. A representative experiment (left) and quantification (right) are *(Figure legend continues)*

Downloaded from http://www.jimmunol.org/ at Institute of Physiology ASCR on April 20, 2021

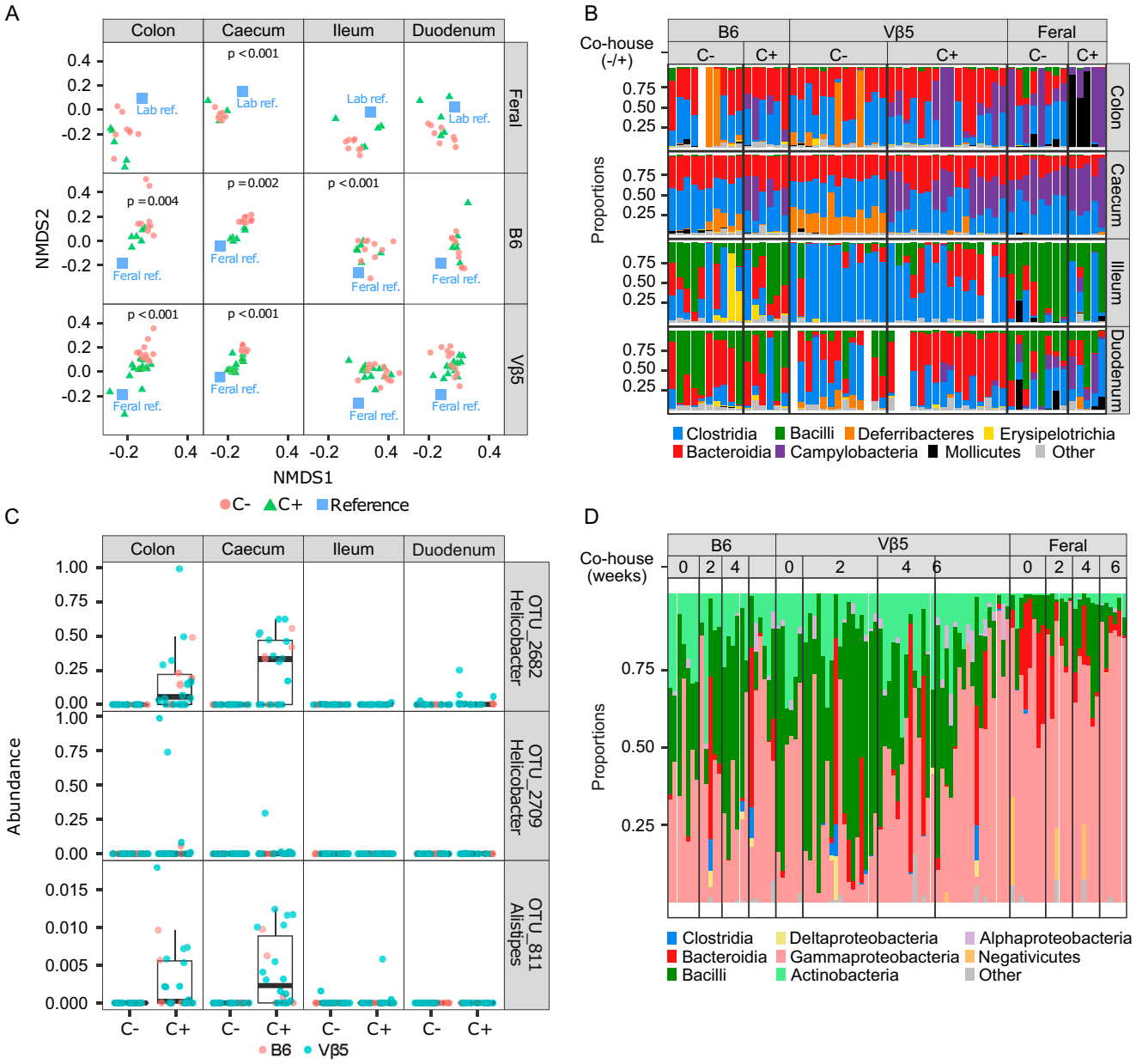

FIGURE 6. Cohousing with feral mice changes the intestinal microbial colonization of laboratory mice. (**A–C**) The analysis of intestinal microbiome of co-housed and non-coshoused laboratory and feral mice (experiment B; see *Materials and Methods*). Samples were taken from the colon, cecum, ileum, or duodenum. C+, coshoused mice for 6 wk (laboratory plus feral); C−, non-cohoused mice. (A) Compositional variation in cohoused versus non-cohoused groups assessed based on Nonmetric Multidimensional Scaling (NMDS) of Bray–Curtis dissimilarities. Centroids for a reference group (feral non-cohoused mice in the case B6 or Vβ5 and non-cohoused Vβ5 plus B6 in the case of feral mice) are indicated by blue rectangles. Permutation-based *p* values indicate significant changes due to co-housing. (B) Taxonomical composition of the intestinal microbiota of laboratory cohoused (C+) and non-cohoused (C−) B6, Vβ5, and feral mice. Color bars represent proportions of dominant bacterial classes in each sample. White space means no data. (C) Three most abundant operational taxonomic units with higher relative abundance in cohoused rather than non-cohoused B6 and Vβ5 laboratory mice. (**D**) Taxonomical composition of the salivary microbiota of laboratory B6 or Vβ5 mice cohoused with feral mice (experiment B; see *Materials and Methods*). Color bars represent proportions of dominant bacterial classes in each sample. Samples were collected from each mouse prior to the cohousing (0 wk) and 2, 4, and 6 wk after the cohousing was set up.

during but not before cohousing (Fig. 6D, Supplemental Fig. 4F). Overall, these data document that cohousing with feral mice changed the microbial colonization of laboratory mice without a substantial impact on the $CD8^+$ T cell compartment.

Discussion

AIMT cells represent one of the two most numerous populations of $CD8^+$ T cells in mice. Although it has been shown that these cells are functionally different from naive and AgE memory T cells (6,

shown. Mean is shown. Statistical significance was calculated using two-tailed Mann–Whitney *U* test. Two independent experiments. (I) Percentages of $TCRV\alpha2^+$ T cells among AIMT ($CD44^+$ $CD49d^-$) and naive ($CD44^-$) $CD8^+$ T cells from cohoused (C+) or non-cohoused (C−) Vβ5 mice. A representative experiment (left) and quantification (right) are shown. $n = 5$ (C−) or 9 (C+) mice in two independent experiments. Statistical significance was tested using Kruskal–Wallis test with Dunn multiple comparison posttests. $^*p < 0.05$, $^{**}p < 0.01$.

Downloaded from http://www.jimmunol.org/ at Institute of Physiology ASCR on April 20, 2021

17, 39, 43–46), our understanding of the biology of these cells is incomplete. There are multiple potential reasons why AIMT cells are an underrepresented area of focus. First, multiple ways of AIMT cells formation were proposed involving different cytokines (IL-4, IL-7, and IL-15), different anatomical sites (thymus, secondary lymphoid organs), and different physiological states (experimentally induced lymphopenia, newborn lymphopenia, aging) (1, 2, 4). Second, the phenotypic and functional similarities between particular AIMT cell subsets and their differences are not well understood (1, 2, 4). Third, only a minority of studies used germ-free mice to exclude microbial Ags (16, 17), and at the same time, no previous study addressed the presence of AIMT cells in feral mice, which were reported to have a substantially different $CD8^+$ T cell compartment than laboratory mice (18).

In this study, we performed comprehensive phenotyping of AIMT cells to address multiple unresolved questions concerning their origin and heterogeneity. We concluded that the formation of AIMT cells represents a robust genetic differentiation program across the genetic background, aging, and hygienic status. However, these three conditions regulate AIMT cell abundance and internal variability.

We identified CD122 as a marker discriminating $CD122^{LOW}$ thymic (innate memory) and peripheral $CD122^{HIGH}$ (virtual memory) subsets of $CD8^+$ AIMT cells. $CD122^{LOW}$ AIMT cells prevail in WT young BALB mice and some feral mice. On the contrary, $CD122^{HIGH}$ AIMT cells are dominant in B6, in some feral mice, and BALB mice with the impaired formation of $CD122^{LOW}$ cells because of aging, expression of a transgenic TCR, disabling the formation of IL-4–producing iNKT cells, or irradiation. Collectively, our data indicate that the absence of thymic innate memory AIMT cells allows the conversion of naive T cells into AIMT cells in the periphery, presumably via IL-4, IL-7, and/or IL-15 (1, 4, 7, 11, 12).

AIMT cells represent the largest population of $CD8^+$ T cells in aged B6 mice (35). In this study, we confirmed this observation in germ-free conditions and extended it by the analysis of aged BALB mice. The mechanism behind the high frequency of AIMT cells in aged animals was unclear. It has been proposed that the origin of these cells might differ from the AIMT cells in young animals (37). We addressed this question by analyzing gene expression profiles and TCR profiling of young and aged AIMT cells using high-throughput sequencing. We observed that AIMT cells show a common gene expression pattern, largely irrespective of their site of origin, genetic background, and the age of the host. However, our analysis revealed that the site of origin and aging fine-tune the gene expression among AIMT cells. In addition to confirming differences between AIMT cells from young and aged B6 mice as reported previously (36), we identified similarities between $CD122^{HIGH}$ AIMT cells from aged BALB mice and AIMT cells from B6 mice. These similarities support the concept that $CD122^{HIGH}$ AIMT cells are formed at the periphery in both B6 and BALB strains. Expression of key effector molecules involved in bystander cytotoxicity as well as IL-12/IL-18 production of IFN-γ was higher in peripheral AIMT cells than in thymic AIMT cells, suggesting that these two subsets differ in their ability to elicit bystander protective immunity, as proposed previously (2). Despite these relatively subtle differences, virtual memory T cells, mostly present in B6 mice, and innate memory T cells, mostly present in young BALB mice, exhibit a very similar gene expression pattern and likely represent two flavors of the AIMT cell lineage.

It has been proposed that aged AIMT cells are formed from T cell clones with a high level of self-reactivity (47). Recently, we have shown that AIMT cells are formed from highly self-reactive T cell clones in young adult mice (17), which was subsequently confirmed by another study (8). In line with these previous reports, we observed that $CD8^+$ naive and AIMT cells use different TCR repertoires. Clones typically present in the naive population are virtually absent in AIMT cells, whereas typical AIMT clones can still be identified in the naive compartment, albeit with a much lower frequency. This partial overlap is not surprising, as AIMT cells are formed from naive T cells in the periphery. However, a recent study by Miller et al. (8) showed a clear separation of naive and AIMT cell repertoires. This discrepancy might be caused by the difference between the employed mouse models. We analyzed TCR $V\alpha2^+$ repertoire in transgenic mice expressing TCR Vβ5 adopted from H2-K^b–restricted OT-I TCR. Importantly, the Vβ5 mouse has a similar frequency of AIMT cells as WT B6 mice. Miller et al. (8) analyzed TCRα repertoire from mice expressing TCR Vβ3-chain. This particular TCRβ chain is abundant among prostate cancer–infiltrating regulatory $CD4^+$ T cells (48) and might produce a T cell repertoire biased toward MHC class II restriction, subsequently affecting the frequency, repertoire, or phenotype of $CD8^+$ AIMT cells.

We observed that young and aged AIMT cells have comparable TCRVα2 repertoire with identical dominant T cell clones and similar level of diversity. Moreover, we observed that AIMT cells preferentially use Vα2 over Vα8.3 TCR chains, which are more pronounced in aged mice. Thus, it is likely that some minor, relatively less self-reactive clonotypes are removed from the AIMT cell repertoire during aging, which is consistent with a previous report (49).

Overall, the probable causes of the high frequency of AIMT cells in aged B6 and BALB mice are as follows: 1) low thymic egress of fresh naive T cells, 2) irreversible AIMT cells formation from highly self-reactive clones augmented by age-related lymphopenia, and 3) the survival and proliferative advantage of AIMT cells over naive T cells.

For the first time, to our knowledge, we studied AIMT cells in feral mice and F1 offspring of feral mice born in captivity, suggesting that AIMT cells are not an artifact of inbred strains and/or SPF conditions. Feral mice showed an even higher frequency of AIMT cells than laboratory strains. This could be caused by the enhancement of the AIMT cell compartment via IL-4 produced in response to helminth (43, 44) or other infections. Indeed, we observed a positive correlation between the frequency of AIMT cells and the percentage of $CD122^{HIGH}$ cells among AIMT cells in feral mice but not in feral F1 offspring born in captivity. This suggests a role of environmentally transient bacterial or helminth infections in feral mice and highlight the role of genetic background in housed F1 offspring.

Although it has been shown that cohousing of laboratory strains with pet shop mice leads to dramatic changes of their $CD8^+$ T cell compartment (18), we could detect only a minor increase of $CX3CR1^+$ effector cells in cohoused B6 mice. Otherwise, the $CD8^+$ T cell compartment in the spleen, peripheral lymph nodes, and mesenteric lymph nodes of cohoused mice was unaffected. A possible explanation is that our feral mice showed much lower pathogenic burden than the pet shop mice used by Beura et al. (18), which seems logical, given the high animal density and the lack of natural predation at pet shop farms. Although different populations of feral mice might have a different pathogenic burden, our data document that cohousing with feral mice does not always induce dramatic changes in the $CD8^+$ T cell compartment. We observed that cohousing with feral mice substantially changes the microbial composition of the intestine and saliva of laboratory strains, including opportunistic pathogens such as *Pasteurella* and *Helicobacter*.

Altogether, our data document that AIMT cells represent a large $CD8^+$ T cell compartment in mice that is present in germ-free as well as in feral conditions. The frequency of peripherally induced self-reactive $CD122^{HIGH}$ AIMT cells increases during aging via homeostatic mechanisms in BALB and B6 mice.

Acknowledgments

We thank Ladislav Cupak for technical assistance and genotyping of mice, Sarka Kocourkova for preparation of RNA-sequencing libraries, Prof. Sai

Downloaded from http://www.jimmunol.org/ at Institute of Physiology ASCR on April 20, 2021

Reddy and Dr. Simon Friedensohn (both from ETH Zürich) for valuable help with designing the assays for TCR repertoire analysis, and Dr. Dominik Filipp (Institute of Molecular Genetics, Prague, Czech Republic) for providing DO11.10 transgenic mice.

Disclosures

The authors have no financial conflicts of interest.

References

1. Pribikova, M., A. Moudra, and O. Stepanek. 2018. Opinion: virtual memory CD8 T cells and lymphopenia-induced memory CD8 T cells represent a single subset: Homeostatic memory T cells. *Immunol. Lett.* 203: 57–61.
2. White, J. T., E. W. Cross, and R. M. Kedl. 2017. Antigen-inexperienced memory CD8$^+$ T cells: where they come from and why we need them. *Nat. Rev. Immunol.* 17: 391–400.
3. Weinreich, M. A., O. A. Odumade, S. C. Jameson, and K. A. Hogquist. 2010. T cells expressing the transcription factor PLZF regulate the development of memory-like CD8+ T cells. *Nat. Immunol.* 11: 709–716.
4. Jameson, S.C., Y.J. Lee, and K.A. Hogquist. 2015. *Innate memory T cells. Adv. Immunology.* 126: 173–213.
5. Tripathi, P., S. C. Morris, C. Perkins, A. Sholl, F. D. Finkelman, and D. A. Hildeman. 2016. IL-4 and IL-15 promotion of virtual memory CD8$^+$ T cells is determined by genetic background. *Eur. J. Immunol.* 46: 2333–2339.
6. White, J. T., E. W. Cross, M. A. Burchill, T. Danhorn, M. D. McCarter, H. R. Rosen, B. O'Connor, and R. M. Kedl. 2016. Virtual memory T cells develop and mediate bystander protective immunity in an IL-15-dependent manner. *Nat. Commun.* 7: 11291.
7. Sosinowski, T., J. T. White, E. W. Cross, C. Haluszczak, P. Marrack, L. Gapin, and R. M. Kedl. 2013. CD8α+ dendritic cell trans presentation of IL-15 to naive CD8+ T cells produces antigen-inexperienced T cells in the periphery with memory phenotype and function. *J. Immunol.* 190: 1936–1947.
8. Miller, C. H., D. E. J. Klawon, S. Zeng, V. Lee, N. D. Socci, and P. A. Savage. 2020. Eomes identifies thymic precursors of self-specific memory-phenotype CD8$^+$ T cells. *Nat. Immunol.* 21: 567–577.
9. Hussain, T., and K. M. Quinn. 2019. Similar but different: virtual memory CD8 T cells as a memory-like cell population. *Immunol. Cell Biol.* 97: 675–684.
10. Smith, N. L., R. K. Patel, A. Reynaldi, J. K. Grenier, J. Wang, N. B. Watson, K. Nzingha, K. J. Yee Mon, S. A. Peng, A. Grimson, et al. 2018. Developmental origin governs CD8$^+$ T cell fate decisions during infection. *Cell* 174: 117–130.e14.
11. Goldrath, A. W., P. V. Sivakumar, M. Glaccum, M. K. Kennedy, M. J. Bevan, C. Benoist, D. Mathis, and E. A. Butz. 2002. Cytokine requirements for acute and basal homeostatic proliferation of naive and memory CD8+ T cells. *J. Exp. Med.* 195: 1515–1522.
12. Goldrath, A. W., L. Y. Bogatzki, and M. J. Bevan. 2000. Naive T cells transiently acquire a memory-like phenotype during homeostasis-driven proliferation. *J. Exp. Med.* 192: 557–564.
13. Kurzweil, V., A. LaRoche, and P. M. Oliver. 2014. Increased peripheral IL-4 leads to an expanded virtual memory CD8+ population. *J. Immunol.* 192: 5643–5651.
14. Kieper, W. C., J. T. Tan, B. Bondi-Boyd, L. Gapin, J. Sprent, R. Ceredig, and C. D. Surh. 2002. Overexpression of interleukin (IL)-7 leads to IL-15-independent generation of memory phenotype CD8+ T cells. *J. Exp. Med.* 195: 1533–1539.
15. Leonard, W. J., J. X. Lin, and J. J. O'Shea. 2019. The γ_c family of cytokines: basic biology to therapeutic ramifications. *Immunity* 50: 832–850.
16. Haluszczak, C., A. D. Akue, S. E. Hamilton, L. D. Johnson, L. Pujanauski, L. Teodorovic, S. C. Jameson, and R. M. Kedl. 2009. The antigen-specific CD8+ T cell repertoire in unimmunized mice includes memory phenotype cells bearing markers of homeostatic expansion. *J. Exp. Med.* 206: 435–448.
17. Drobek, A., A. Moudra, D. Mueller, M. Huranova, V. Horkova, M. Pribikova, R. Ivanek, S. Oberle, D. Zehn, K. D. McCoy, et al. 2018. Strong homeostatic TCR signals induce formation of self-tolerant virtual memory CD8 T cells. *EMBO J.* 37: e98518.
18. Beura, L. K., S. E. Hamilton, K. Bi, J. M. Schenkel, O. A. Odumade, K. A. Casey, E. A. Thompson, K. A. Fraser, P. C. Rosato, A. Filali-Mouhim, et al. 2016. Normalizing the environment recapitulates adult human immune traits in laboratory mice. *Nature* 532: 512–516.
19. Fink, P. J., K. Swan, G. Turk, M. W. Moore, and F. R. Carbone. 1992. Both intrathymic and peripheral selection modulate the differential expression of V beta 5 among CD4+ and CD8+ T cells. *J. Exp. Med.* 176: 1733–1738.
20. Murphy, K. M., A. B. Heimberger, and D. Y. Loh. 1990. Induction by antigen of intrathymic apoptosis of CD4+CD8+TCRlo thymocytes in vivo. *Science* 250: 1720–1723.
21. Zerbino, D. R., P. Achuthan, W. Akanni, M. R. Amode, D. Barrell, J. Bhai, K. Billis, C. Cummins, A. Gall, C. G. Girón, et al. 2018. Ensembl 2018. *Nucleic Acids Res.* 46(D1): D754–D761.
22. Kim, D., B. Langmead, and S. L. Salzberg. 2015. HISAT: a fast spliced aligner with low memory requirements. *Nat. Methods* 12: 357–360.
23. Liao, Y., G. K. Smyth, and W. Shi. 2014. featureCounts: an efficient general purpose program for assigning sequence reads to genomic features. *Bioinformatics* 30: 923–930.
24. Love, M. I., W. Huber, and S. Anders. 2014. Moderated estimation of fold change and dispersion for RNA-seq data with DESeq2. *Genome Biol.* 15: 550.
25. Stephens, M. 2017. False discovery rates: a new deal. *Biostatistics* 18: 275–294.
26. Ritchie, M. E., B. Phipson, D. Wu, Y. Hu, C. W. Law, W. Shi, and G. K. Smyth. 2015. Limma powers differential expression analyses for RNA-sequencing and microarray studies. *Nucleic Acids Res.* 43: e47.
27. Shugay, M., O. V. Britanova, E. M. Merzlyak, M. A. Turchaninova, I. Z. Mamedov, T. R. Tuganbaev, D. A. Bolotin, D. B. Staroverov, E. V. Putintseva, K. Plevova, et al. 2014. Towards error-free profiling of immune repertoires. *Nat. Methods* 11: 653–655.
28. Klindworth, A., E. Pruesse, T. Schweer, J. Peplies, C. Quast, M. Horn, and F. O. Glöckner. 2013. Evaluation of general 16S ribosomal RNA gene PCR primers for classical and next-generation sequencing-based diversity studies. *Nucleic Acids Res.* 41: e1.
29. Glenn, T. C., R. A. Nilsen, T. J. Kieran, J. G. Sanders, N. J. Bayona-Vásquez, J. W. Finger, T. W. Pierson, K. E. Bentley, S. L. Hoffberg, S. Louha, et al. 2019. Adapterama I: universal stubs and primers for 384 unique dual-indexed or 147,456 combinatorially-indexed Illumina libraries (iTru & iNext). *PeerJ.* 7: e7755.
30. Jiang, H., R. Lei, S. W. Ding, and S. Zhu. 2014. Skewer: a fast and accurate adapter trimmer for next-generation sequencing paired-end reads. *BMC Bioinformatics* 15: 182.
31. Callahan, B. J., P. J. McMurdie, M. J. Rosen, A. W. Han, A. J. Johnson, and S. P. Holmes. 2016. DADA2: High-resolution sample inference from Illumina amplicon data. *Nat. Methods* 13: 581–583.
32. Edgar, R. C., B. J. Haas, J. C. Clemente, C. Quince, and R. Knight. 2011. UCHIME improves sensitivity and speed of chimera detection. *Bioinformatics* 27: 2194–2200.
33. Wang, Q., G. M. Garrity, J. M. Tiedje, and J. R. Cole. 2007. Naive Bayesian classifier for rapid assignment of rRNA sequences into the new bacterial taxonomy. *Appl. Environ. Microbiol.* 73: 5261–5267.
34. Quast, C., E. Pruesse, P. Yilmaz, J. Gerken, T. Schweer, P. Yarza, J. Peplies, and F. O. Glöckner. 2013. The SILVA ribosomal RNA gene database project: improved data processing and web-based tools. *Nucleic Acids Res.* 41(Database issue, D1)D590–D596.
35. Chiu, B. C., B. E. Martin, V. R. Stolberg, and S. W. Chensue. 2013. Cutting edge: central memory CD8 T cells in aged mice are virtual memory cells. *J. Immunol.* 191: 5793–5796.
36. Quinn, K. M., A. Fox, K. L. Harland, B. E. Russ, J. Li, T. H. O. Nguyen, L. Loh, M. Olshanksy, H. Naeem, K. Tsyganov, et al. 2018. Age-related decline in primary CD8$^+$ T cell responses is associated with the development of senescence in virtual memory CD8$^+$ T cells. *Cell Rep.* 23: 3512–3524.
37. Renkema, K. R., G. Li, A. Wu, M. J. Smithey, and J. Nikolich-Žugich. 2014. Two separate defects affecting true naive or virtual memory T cell precursors combine to reduce naive T cell responses with aging. *J. Immunol.* 192: 151–159.
38. Decman, V., B. J. Laidlaw, T. A. Doering, J. Leng, H. C. Ertl, D. R. Goldstein, and E. J. Wherry. 2012. Defective CD8 T cell responses in aged mice are due to quantitative and qualitative changes in virus-specific precursors. *J. Immunol.* 188: 1933–1941.
39. Lanzer, K. G., T. Cookenham, W. W. Reiley, and M. A. Blackman. 2018. Virtual memory cells make a major contribution to the response of aged influenza-naïve mice to influenza virus infection. [Published erratum appears in 2018 Immun. Ageing 15:18.] *Immun. Ageing* 15: 17.
40. Robertson, J. M., P. E. Jensen, and B. D. Evavold. 2000. DO11.10 and OT-II T cells recognize a C-terminal ovalbumin 323-339 epitope. *J. Immunol.* 164: 4706–4712.
41. Akue, A. D., J. Y. Lee, and S. C. Jameson. 2012. Derivation and maintenance of virtual memory CD8 T cells. *J. Immunol.* 188: 2516–2523.
42. Daniels, M. A., and E. Teixeiro. 2020. Forget 'ME' not virtual memory T cells. *Nat. Immunol.* 21: 499–500.
43. Lin, J. S., K. Mohrs, F. M. Szaba, L. W. Kummer, E. A. Leadbetter, and M. Mohrs. 2019. Virtual memory CD8 T cells expanded by helminth infection confer broad protection against bacterial infection. *Mucosal Immunol.* 12: 258–264.
44. Rolot, M., A. M. Dougall, A. Chetty, J. Javaux, T. Chen, X. Xiao, B. Machiels, M. E. Selkirk, R. M. Maizels, C. Hokke, et al. 2018. Helminth-induced IL-4 expands bystander memory CD8$^+$ T cells for early control of viral infection. *Nat. Commun.* 9: 4516.
45. Lee, J. Y., S. E. Hamilton, A. D. Akue, K. A. Hogquist, and S. C. Jameson. 2013. Virtual memory CD8 T cells display unique functional properties. *Proc. Natl. Acad. Sci. USA* 110: 13498–13503.
46. Grau, M., S. Valsesia, J. Mafille, S. Djebali, M. Tomkowiak, A. L. Mathieu, D. Laubreton, S. de Bernard, P. E. Jouve, E. Ventre, et al. 2018. Antigen-induced but not innate memory CD8 T cells express NKG2D and are recruited to the lung parenchyma upon viral infection. *J. Immunol.* 200: 3635–3646.
47. Rudd, B. D., V. Venturi, G. Li, P. Samadder, J. M. Ertelt, S. S. Way, M. P. Davenport, and J. Nikolich-Žugich. 2011. Nonrandom attrition of the naive CD8+ T-cell pool with aging governed by T-cell receptor:pMHC interactions. *Proc. Natl. Acad. Sci. USA* 108: 13694–13699.
48. Malchow, S., D. S. Leventhal, S. Nishi, B. I. Fischer, L. Shen, G. P. Paner, A. S. Amit, C. Kang, J. E. Geddes, J. P. Allison, et al. 2013. Aire-dependent thymic development of tumor-associated regulatory T cells. *Science* 339: 1219–1224.
49. Quinn, K. M., S. G. Zaloumis, T. Cukalac, W. T. Kan, X. Y. Sng, M. Mirams, K. A. Watson, J. M. McCaw, P. C. Doherty, P. G. Thomas, et al. 2016. Heightened self-reactivity associated with selective survival, but not expansion, of naïve virus-specific CD8+ T cells in aged mice. *Proc. Natl. Acad. Sci. USA* 113: 1333–1338.

Downloaded from http://www.jimmunol.org/ at Institute of Physiology ASCR on April 20, 2021

Figure S1

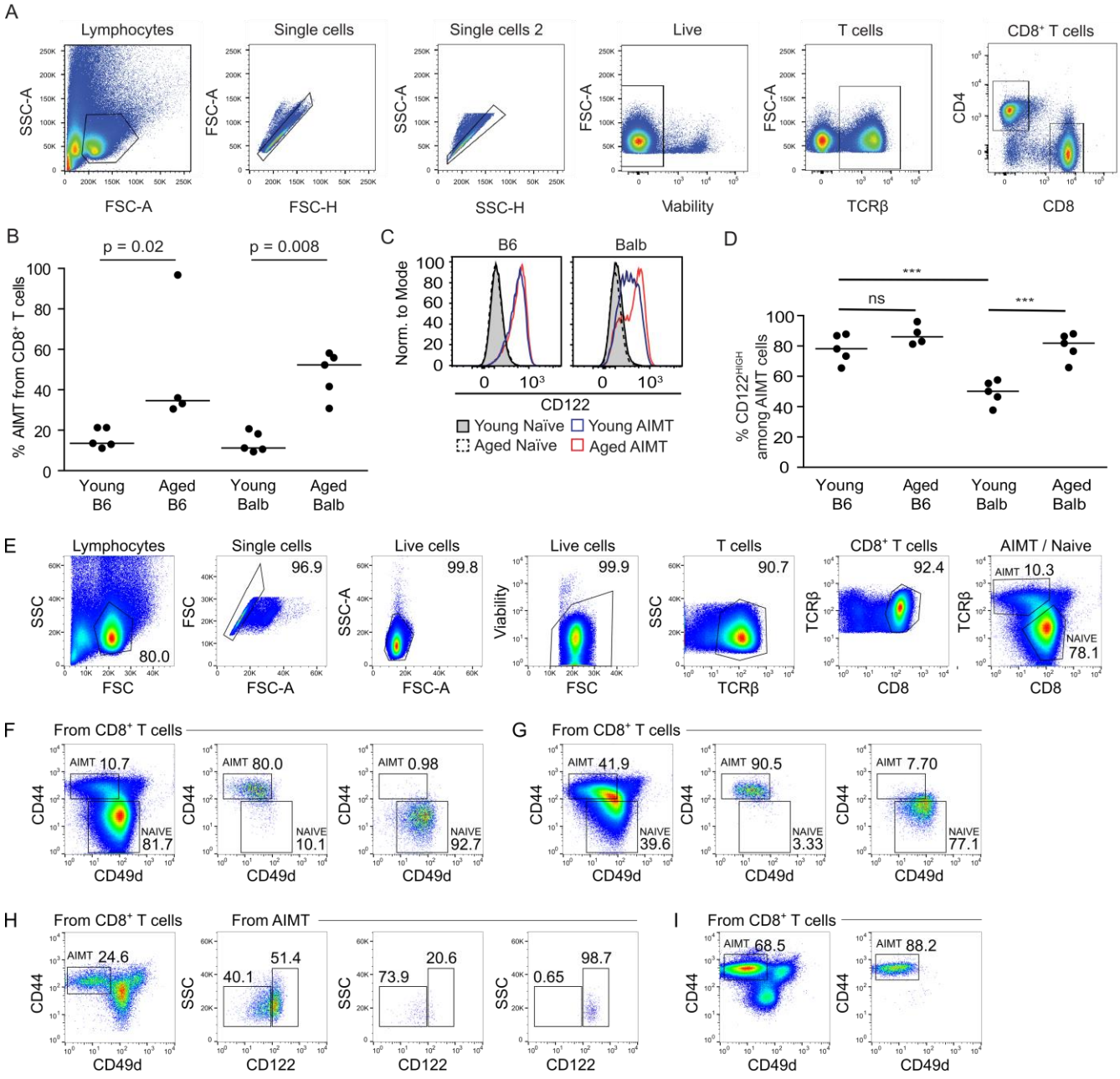
A
Lymphocytes
Single cells
Single cells 2
Live
T cells
CD8⁺ T cells
SSC-A
FSC-A
FSC-H
SSC-H
Viability
TCRβ
CD4
CD8
B
p = 0.02
p = 0.008
% AIMT from CD8⁺ T cells
Young B6
Aged B6
Young Balb
Aged Balb
C
B6
Balb
Norm. to Mode
CD122
Young Naïve
Young AIMT
Aged Naïve
Aged AIMT
D
ns
***
% CD122HIGH among AIMT cells
E
Lymphocytes
Single cells
Live cells
Live cells
T cells
CD8⁺ T cells
AIMT / Naive
80.0
96.9
99.8
99.9
90.7
92.4
AIMT 10.3
NAIVE 78.1
SSC
FSC
FSC-A
SSC-A
Viability
TCRβ
CD8
F
From CD8⁺ T cells
AIMT 10.7
NAIVE 81.7
AIMT 80.0
NAIVE 10.1
AIMT 0.98
NAIVE 92.7
CD44
CD49d
G
From CD8⁺ T cells
AIMT 41.9
NAIVE 39.6
AIMT 90.5
NAIVE 3.33
AIMT 7.70
NAIVE 77.1
H
From CD8⁺ T cells
From AIMT
AIMT 24.6
40.1
51.4
73.9
20.6
0.65
98.7
SSC
CD122
I
From CD8⁺ T cells
AIMT 68.5
AIMT 88.2

Supplemental Figure 1.

(A) Gating strategy for gating of $CD8^+$ T cells in the flow cytometry experiments shown in this study.

(B-D) Analysis of lymph nodes from the same mice as in the experiments in Figure 1A-D. Median.

(B) Quantification of the percentage of $CD44^+$ $CD49d^-$ AIMT cells among CD8 T cells. n=4 (Balb) or 5 (B6) mice from 2-5 independent experiments. The statistical significance was tested using 2-tailed Mann-Whitney test.

(C) Histograms of CD122 expression in $CD44^-$ naïve and $CD44^+$ $CD49d^-$ AIMT cells from indicated mice. A representative experiment out of two in total.

(D) Quantification of $CD122^{HIGH}$ cells among $CD8^+$ AIMT cells. Median. The statistical significance was tested using 1-way ANOVA ($p < 0.0001$) with Bonferroni's Multiple Comparison (post)Tests. *** $p \leq 0.001$.

(E-I) Gating strategies and re-analyses for cell sorting for the mRNA sequencing experiment shown in Fig 3. Representative samples per condition out of 3 in total are shown.

(E) General gating strategy for gating AIMT/Naïve $CD8^+$ T cells for sorting.

(F-G) Naïve and AIMT cell gates for pre-sorted cells (left) and re-analyses of the sorted samples (AIMT – center, Naïve – right) from young B6 (F) or Balb (G) mice.

(H) AIMT cell gate for pre-sorted cells in aged Balb mice (1^{st} panel from the left). Sorting gate (2^{nd} panel) and re-analyses of the sorted samples from aged Balb mice (3^{rd} panel – $CD122^{LOW}$ AIMT, 4^{th} panel –$CD122^{HIGH}$ AIMT).

(I) AIMT cell gate for pre-sorted cells (left) and re-analysis (right) of the sorted sample from aged B6 mice.

Figure S2

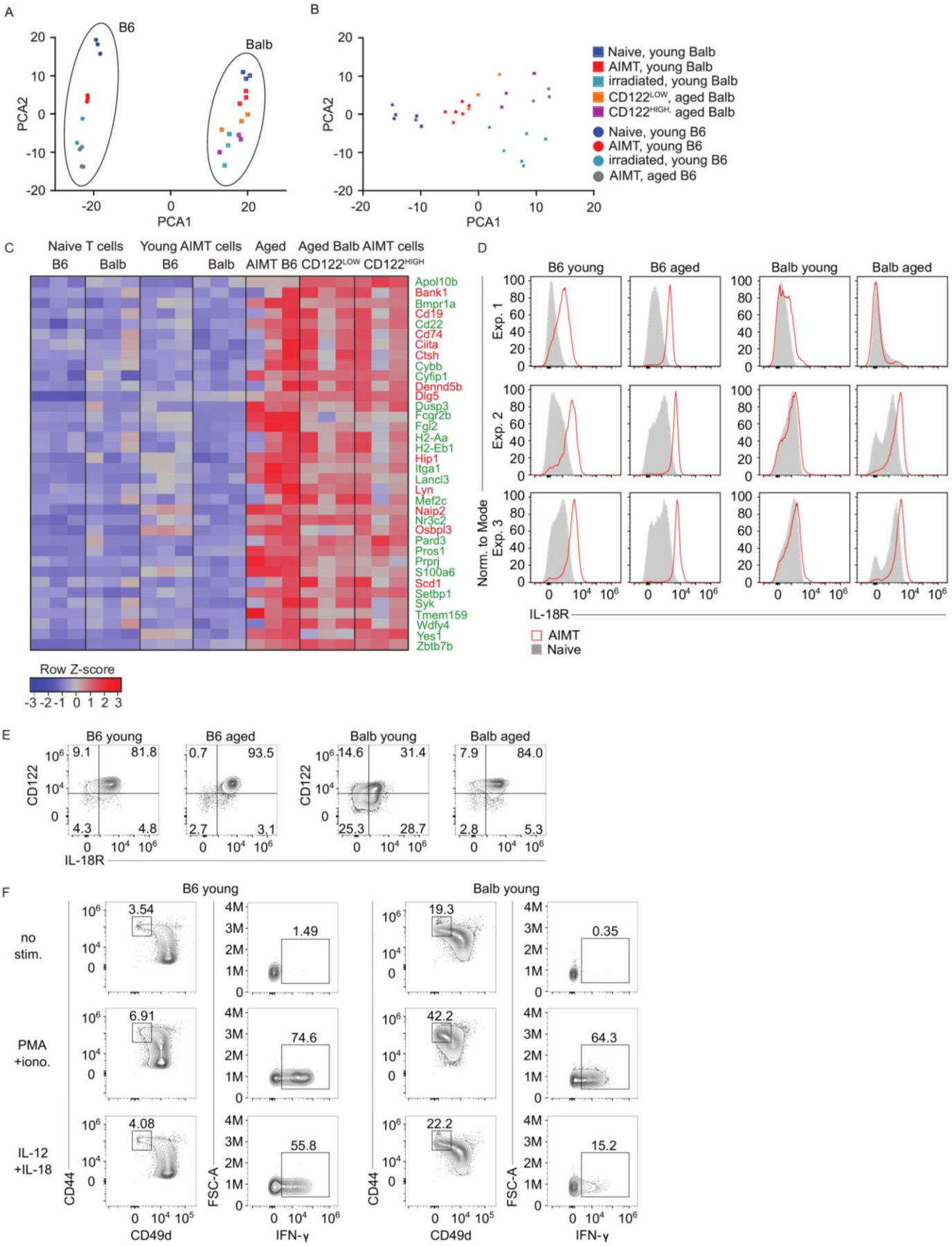
A
B6
Balb
PCA2
PCA1
B
Naive, young Balb
AIMT, young Balb
irradiated, young Balb
CD122LOW, aged Balb
CD122HIGH, aged Balb
Naive, young B6
AIMT, young B6
irradiated, young B6
AIMT, aged B6
C
Naive T cells
Young AIMT cells
Aged AIMT B6
Aged Balb AIMT cells
B6
Balb
CD122LOW
CD122HIGH
Apol10b
Bank1
Bmpr1a
Cd19
Cd22
Cd74
Ciita
Ctsh
Cybb
Cyfip1
Dennd5b
Dlg5
Dusp3
Fcgr2b
Fgl2
H2-Aa
H2-Eb1
Hip1
Itga1
Lancl3
Lyn
Mef2c
Naip2
Nr3c2
Osbpl3
Pard3
Pros1
Prprj
S100a6
Scd1
Setbp1
Syk
Tmem159
Wdfy4
Yes1
Zbtb7b
Row Z-score
D
B6 young
B6 aged
Balb young
Balb aged
Exp. 1
Exp. 2
Exp. 3
Norm. to Mode
IL-18R
AIMT
Naive
E
B6 young
B6 aged
Balb young
Balb aged
CD122
IL-18R
9.1
81.8
4.3
4.8
0.7
93.5
2.7
3.1
14.6
31.4
25.3
28.7
7.9
84.0
2.8
5.3
F
B6 young
Balb young
no stim.
PMA +iono.
IL-12 +IL-18
CD44
CD49d
FSC-A
IFN-γ
3.54
1.49
19.3
0.35
6.91
74.6
42.2
64.3
4.08
55.8
22.2
15.2

Supplemental Figure 2.

(A-B) PCA analysis (top 500 variable genes) of the gene expression profiles of the individual samples (Fig. S1E-I, Fig. 3) prior to the normalization between strains (A) and after removing genes differentially expressed between strains (B).

(C) Heatmap showing relative expression of 36 genes showing significant upregulation in AIMT cells from aged mice in comparison to AIMT cells in young mice in B6 and Balb strains (both in $CD122^{HIGH}$ and $CD122^{LOW}$ AIMT cells from aged Balb mice). Names of genes upregulated in AIMT cells from aged B6 mice in comparison to young B6 mice in the previously published dataset [36] are in green.

(D) Surface levels of IL-18R in naïve and AIMT $CD8^+$ T cells from young and aged Balb and B6 mice measured by flow cytometry. Supplemental histograms for the experiment shown in Fig. 3G. Three independent experiments are shown.

(E) Surface levels of IL-18R and CD122 in AIMT $CD8^+$ T cells from young and aged Balb and B6 mice measured by flow cytometry. A representative experiment out of three in total (same experiments as shown in Figure S2D).

(F) Production of IFN-γ by AIMT cells (gated as $CD8^+$ $CD44^+$ $CD49d^-$) isolated from young B6 or Balb mice measured by flow cytometry. Supplemental representative contour plots for the experiment shown in Fig. 3H. A representative experiment out of three in total (same experiments as shown in Figure S2D).

Figure S3

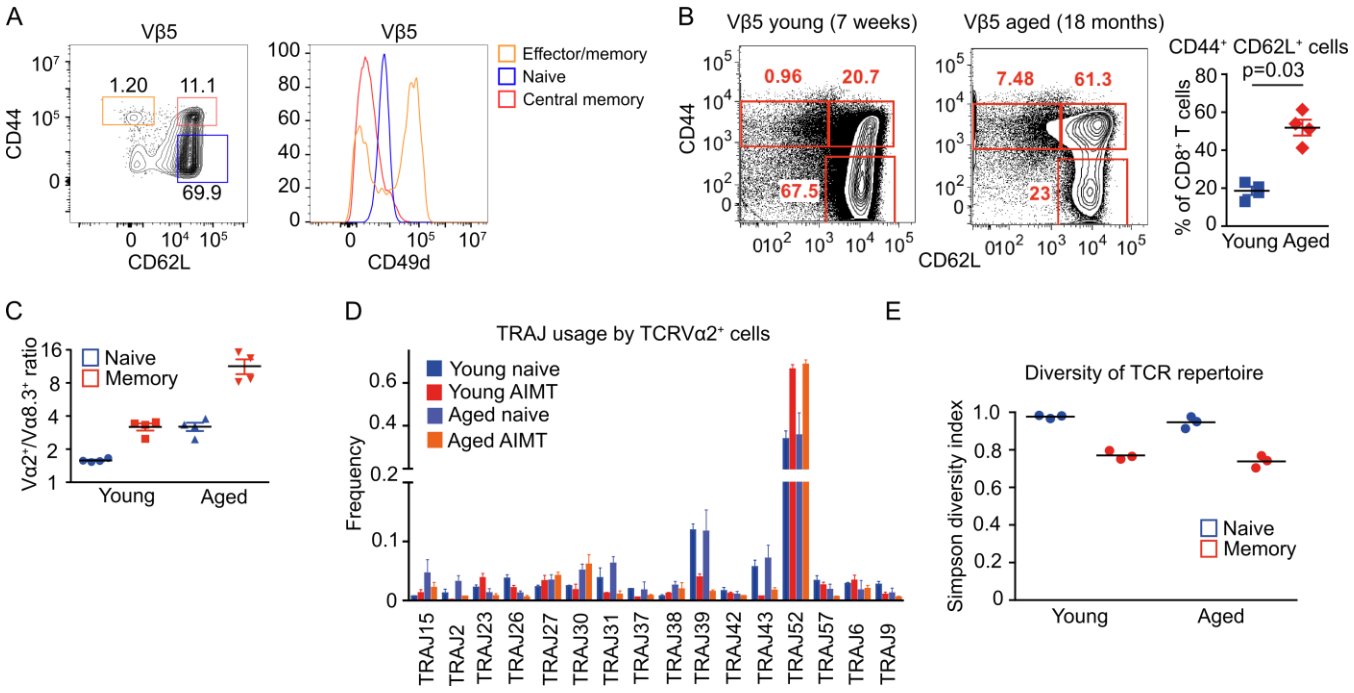

Supplemental Figure 3.

(A) Expression of the CD49d marker on naïve ($CD44^-$ $CD62L^+$), central memory phenotype ($CD44^+$ $CD62L^+$), and effector/memory ($CD44^+$ $CD62L^+$) cells in the lymph nodes of young Vβ5 mice. A representative sample is shown out of 5 independent experiments.

(B-C) Analysis of the same young and aged Vβ5 mice as the experiment in Fig. 4A.

(B) Percentage of naïve ($CD44^-$ $CD62L^+$), AIMT ($CD44^+$ $CD62L^+$), and effector/memory ($CD44^+$ $CD62L^-$) cells in the lymph nodes of young and aged mice. Mean ± SEM is shown. A representative experiment and the quantification of 4 mice per group are shown. Statistical significance was calculated using Mann-Whitney test.

(C) Quantification of the ratio between the TCRVα2 and TCRVα8.3 T cells among AIMT or naïve $CD8^+$ T cells in Vβ5 young or aged mice. Mean ± SEM is shown.

(D) Quantification of the TRAJ usage by the indicated mice. Mean + SEM. Analysis of the same experiment as shown in Fig. 4B-F.

(E) Diversity of the CDR3 among TRAV14 TCRα in naïve and AIMT CD8+ T cells isolated from Vβ5 mice was estimated using Simpson diversity index. Mean is shown. The statistical significance was calculated using one-way ANOVA with Bonferroni's Multiple Comparison Posttest. ns; $p>0.05$. Analysis of the same experiment as shown in Fig. 4B-F.

Figure S4

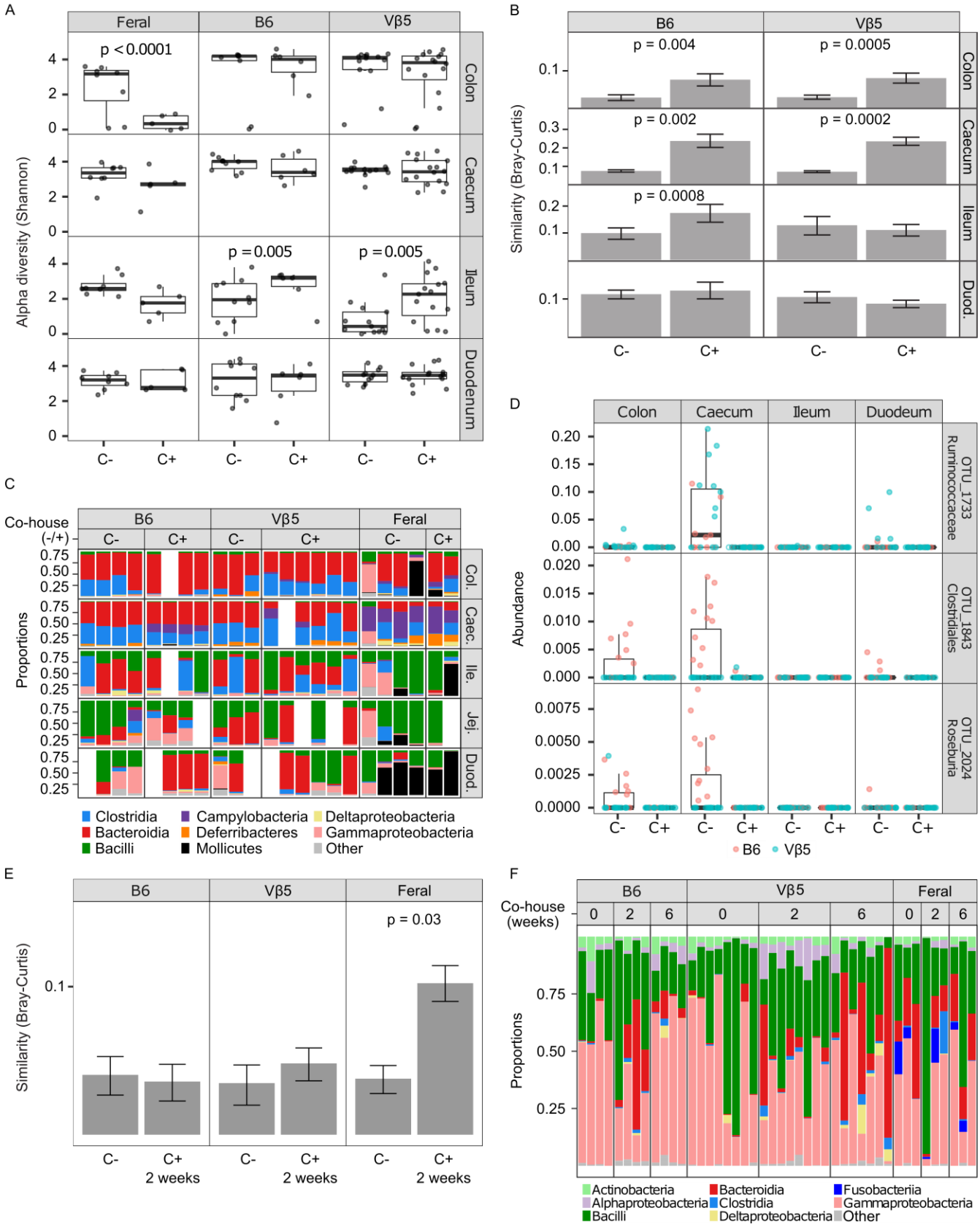
A
Feral
B6
Vβ5
p < 0.0001
p = 0.005
p = 0.005
Colon
Caecum
Ileum
Duodenum
Alpha diversity (Shannon)
C-
C+
B
B6
Vβ5
p = 0.004
p = 0.0005
p = 0.002
p = 0.0002
p = 0.0008
Similarity (Bray-Curtis)
Colon
Caecum
Ileum
Duod.
C
Co-house (-/+)
B6
Vβ5
Feral
Proportions
Col.
Caec.
Ile.
Jej.
Duod.
Clostridia
Bacteroidia
Bacilli
Campylobacteria
Deferribacteres
Mollicutes
Deltaproteobacteria
Gammaproteobacteria
Other
D
Colon
Caecum
Ileum
Duodeum
Abundance
OTU_1733 Ruminococcaceae
OTU_1843 Clostridiales
OTU_2024 Roseburia
B6
Vβ5
E
B6
Vβ5
Feral
p = 0.03
Similarity (Bray-Curtis)
C-
C+
2 weeks
F
B6
Vβ5
Feral
Co-house (weeks)
0
2
6
Proportions
Actinobacteria
Alphaproteobacteria
Bacilli
Bacteroidia
Clostridia
Deltaproteobacteria
Fusobacteriia
Gammaproteobacteria
Other

Supplemental Figure 4.

(A-B) Analysis of the experiment shown in Figure 6A-C.

(A) Shannon-index based alpha diversity of the gut microbiota of feral and laboratory mice co-housed together (C+) or non-co-housed (C-). The statistical significance was tested using linear mixed effect model, while considering individual identity as a random effect and the effect of treatment level (co-housed vs non-co-housed), gut section, and their interactions as explanatory variables.

(B) Average Bray-Curtis similarity score of intestinal microbiota between laboratory B6 or Vβ5 mice co-housed (C+) or non-co-housed (C-) with feral mice and non-co-housed feral mice. Error bars correspond to 95% bootstrap confidence intervals, permutation-based p-values are shown for significant differences ($p < 0.05$). Duod. – Duodenum.

(C) Taxonomical composition of the intestinal microbiota of laboratory co-housed (C+) and non-co-housed (C-) B6, Vβ5, and feral mice (Experiment A, see Methods). Color bars represent proportions of dominant bacterial classes in each sample. Col. – Colon, Caec. – Caecum, Ile. – Ileum, Jej. – Jejunum, Duod. – Duodenum.

(D) Three most abundant operational taxonomic units with lower relative abundance in co-housed (C+) than non-co-housed (C-) B6 and Vβ5 laboratory mice. (Experiment B, see Methods).

(E) Average Bray-Curtis similarity of the salivary microbiota of co-housed (C+) or non-co-housed (C-) laboratory B6 or Vβ5 mice with feral mice to conventional feral mice (left, center), or co-housed or non-co-housed feral mice to laboratory B6 and Vβ5 controls (right) in the experiment shown in Figure 6D. Error bars correspond to 95% bootstrap confidence intervals. Permutation-based p-value is shown for significant differences ($p < 0.05$).

(F) Taxonomical composition of the salivary microbiota of laboratory B6 or Vβ5 mice co-housed vs. non-co-housed with feral mice (Experiment A, see Methods). Color bars represent proportions of dominant bacterial classes in each sample. Samples were collected from each mouse prior to the co-housing (0 weeks) and after 2 and 6 weeks during the co-housing experiment.